Comparison of very long baseline interferometry, GPS, and satellite laser ranging height residuals from ITRF2005 using spectral and correlation methods

X. Collilieux,[1] Z. Altamimi,[1] D. Coulot,[1] J. Ray,[2] and P. Sillard[3]

[1]   For the first time, the ITRF2005 input data are in the form of time series of station positions and Earth orientation parameters, together with full variance-covariance information. The first step of the ITRF2005 analysis consists of rigorously stacking each time series to yield a long-term solution per technique. As a by-product, time series of position residuals contain the nonlinear motion of points over the Earth's surface. In this paper, the height residual time series of very long baseline interferometry (VLBI), Global Positioning System (GPS), and satellite laser ranging (SLR) solutions submitted to ITRF2005 are compared. We note that the interpretation of the ITRF2005 position residual time series as observed physical motions at the various stations is delicate due to the inhomogeneous site distribution. We estimate that the network effect may introduce an averaged scatter of 3 and 2 mm in the VLBI and SLR height residuals, respectively. Although noise levels are different among these three techniques, a common 1.0 cycles per year (cpy) frequency is clearly detected. The GPS height annual signal exhibits significant regional correlations that are confirmed by VLBI and SLR measurements in some colocated sites. Significant power near frequencies 2.00, 3.12, and 4.16 cpy is also detected in the individual GPS height residuals time series as mentioned by Ray et al. (2007). However, neither VLBI nor SLR show any significant signals at these frequencies for colocated sites. The agreement between detrended height time series at colocated sites is quantified using a novel method based on Kalman filtering and on maximum likelihood estimation. The GPS and VLBI measurements are shown to agree fairly well for most of the colocated sites. However, agreement is not generally observed in the GPS and SLR comparisons. A study of the interannual signal at colocated sites indicates that the good correlation cannot be completely attributed to the annual harmonic.

1.   Introduction

[2]   ITRF2005, the newest release of the International Terrestrial Reference Frame (ITRF) as a realization of the International Terrestrial Reference Systems (ITRS) [*McCarthy and Petit*, 2004], is a set of positions and velocities of points located on the Earth's surface. For the first time, it is associated with a set of consistent Earth orientation parameters (EOPs) taking an important step to ensure consistency among the International Earth Rotation and Reference System Service (IERS) products [*Altamimi et al.*, 2007]. As with previous versions, the ITRF2005 solution has been computed using data from the four main space geodetic techniques, very long baseline interferometry (VLBI), satellite laser ranging (SLR), Global Positioning System (GPS) and Doppler orbitography and Radio-positioning Integrated by Satellites (DORIS), together with local ties at colocation sites. The use of these four techniques is essential to take advantage of the strengths of each for the benefit of the combined frame. For the first time, ITRF2005 input data are in the form of time series of station positions and EOPs with their full variance-covariance matrices.

[3]   The strategy adopted for the ITRF2005 combination has two steps [*Altamimi et al.*, 2007]. The first step is the independent computation of a long-term stacked Terrestrial Reference Frame (TRF) for each measurement technique under the assumption of linear motions. A unique set of positions and velocities is computed for every observing station of each technique in a reference system specific to the technique. The associated EOPs are readjusted simultaneously to make them consistent with their stacked TRFs. Thus for each technique the first computation step produces

[1]Laboratoire de Recherche en Géodésie/Institut Géographique National, Marne-La-Vallée, France.
[2]NOAA National Geodetic Survey, Silver Spring, Maryland, USA.
[3]Institut National de la Statistique et des Etudes Economiques, Malakoff, France.

a consistent set of station positions and velocities, and EOPs together with their full covariance matrix. In the second step these individual secular reference frames are combined making use of local intertechnique ties to yield positions and velocities for every point, with time-varying EOPs, in a consistent and well-defined global frame.

[4] The intertechnique combination requires an assessment of the consistency of the long-term site motions given by the various measurement techniques. Beginning with ITRF2005 it is now possible to assess the nonlinear motions through the residuals of the first computational step. We need to investigate what lessons can be learned from their study to improve the secular reference frame combination process and to probe whether technique-dependent systematic errors are detectable. Only the height component is investigated here because most geophysical signals, as well as most systematic errors, are expected to be largest in this component.

[5] Indeed, due mainly to gravitational attraction by celestial bodies, internal mass flows, and various mass redistributions at the Earth's surface between the ground, the atmosphere and the ocean, the Earth's crust is continuously deforming. This deformation is one of the signals that geophysicists wish to measure and understand. One of the main tasks of geodesy is to try to model as accurately as possible all other effects which may contaminate the measurements. Ever since geodetic coordinate repeatability became sufficiently precise to detect predicted loading motion, geodetic measurements have been used to try to validate geodynamical models. Atmospheric pressure and continental water loading have been detected in various studies, using alternatively GPS [*van Dam et al.*, 1994; *van Dam et al.*, 2001], VLBI [*van Dam and Herring*, 1994; *Petrov and Boy*, 2004], or DORIS observations [*Mangiarotti et al.*, 2001]. Most of the time, these studies provide an acceptable agreement between geodetic positioning and theoretical model predictions but the measurements cannot be fully explained by the models. Power spectra of the GPS coordinate time series have been the most widely studied. *Blewitt and Lavallée* [2002] have analyzed the spectral content of GPS height time series and have clearly detected annual and semiannual signals as well as higher harmonics. *Dong et al.* [2002] tried to explain the significant annual and semiannual ("seasonal") signals in GPS height time series by investigating all possible individual contributions; less than half of the observed seasonal motion can be explained by known loading effects. More recently, *van Dam et al.* [2007] have compared GPS height residual time series to GRACE gravity field observation over Europe, and show that the agreement is not yet achieved. According to *Titov and Yakovleva* [1999], annual signals have been also detected in VLBI baseline length time series; a semiannual signature has also been identified for some baselines. A more complete study has been led by *Petrov and Ma* [2003]: The motion of every VLBI telescope has been modeled by sums of harmonics whose terms have been estimated simultaneously from the time delay observations. Significant annual signals have been detected and partly attributed to hydrological loading. *Petrov and Ma* [2003] also revealed that VLBI annual vertical motions are positively correlated with the annual motion measured by colocated GPS observations from *Dong et al.* [2002]. *Ding*

et al. [2005] have also compared GPS and VLBI computed time series at colocated sites. Their wavelet analysis of the half-monthly sampled GPS and VLBI time series exhibits signals with time-varying amplitudes. The annual signal was in phase for both techniques but exhibited higher amplitude for GPS. Interannual signals have also been proved to be correlated for most of the considered colocated sites. Fewer studies have been conducted concerning nonlinear motions in SLR position time series. More recently, *Ray et al.* [2007] have analyzed the general spectral content of these three techniques by computing stacked periodograms of the ITRF2005 position residuals and loading displacement models. They have emphasized that GPS station positions contain harmonics of the 1.04 cpy frequency, up to the sixth.

[6] These previous studies have emphasized that only a part of the displacement observed could be attributed to the real motion of the ground. Systematic errors may degrade the observed displacements, notably on the height component. Indeed, any nonmodeled or mismodeled contribution affecting the range measurements or the station a priori motions can contribute to the station position time series scattering. Also, as shown by *Stewart et al.* [2005], the impact of unmodeled tidal signals in the geodetic observation processing can cause aliasing into longer-period signals. Thus each space geodetic technique acts as a filter of the measurements, creating its own artifact signals.

[7] Here, we aim at comparing the height measurements provided by GPS, SLR and VLBI which are known to have the best internal precision [*Altamimi et al.*, 2007]. This intertechnique comparison aims at detecting possible individual technique systematic errors with the limitation that any common systematic error will not be detected. This work is an assessment, at the time of the ITRF2005 release, of the agreement in the height estimates among the three techniques. The input time series span more than 10 common years, with continuously weekly samplings for GPS and SLR, and irregular 24-h intervals for VLBI. We have analyzed these three solutions to separate the nonlinear motion of individual points from the global motion and biases that affect the whole set of stations. Unfortunately, this procedure cannot be fully realized since station displacements may alias into the global parameters. We have consequently evaluated the possible error introduced. The comparison of the derived height residuals is then achieved in two main steps. The spectral contents of the height residual time series are first investigated to search for significant common spectral lines in the data sets. The study then focuses on the annual signal which is the most significant common spectral line. Next, we develop a method based on Kalman filtering and maximum likelihood estimation (MLE) to assess height time series similarities and compute correlation coefficients. This method is applied to height time series for sites with sufficient common data spans from multiple techniques.

2. ITRF2005 Data Processing

[8] ITRF2005 input solutions using SLR, VLBI, and GPS have been analyzed by the geodetic services of the International Association of Geodesy (IAG): the International Laser Ranging Service (ILRS), the International VLBI
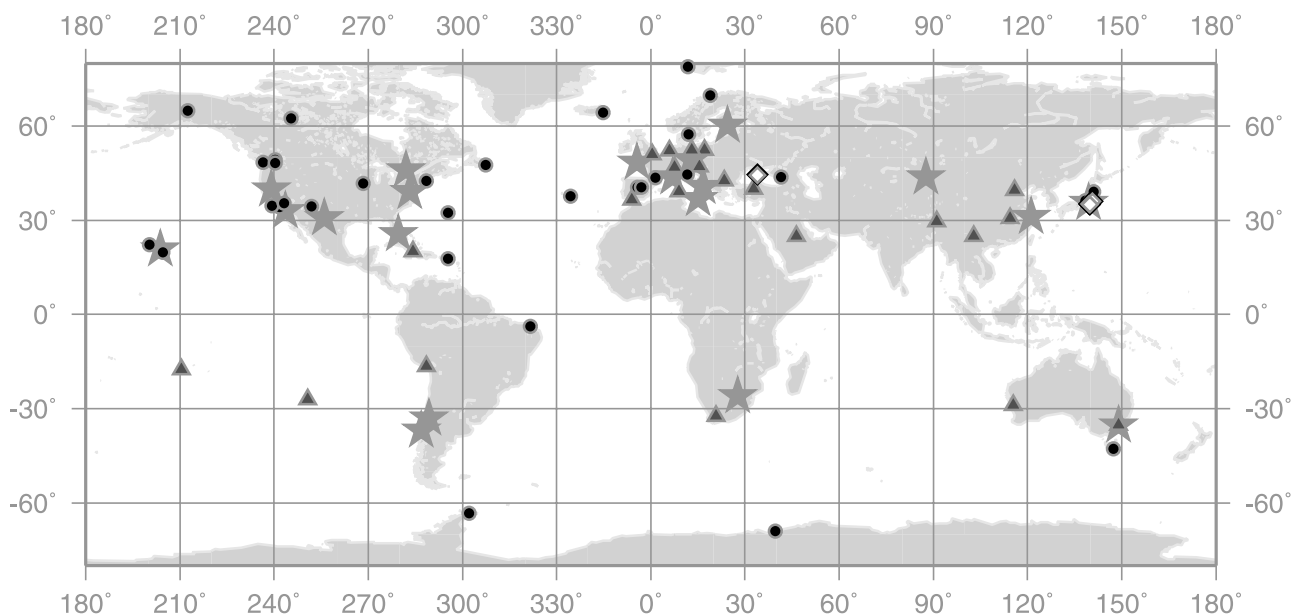
Figure 1. GPS, VLBI and SLR colocated sites of ITRF2005. Star, GPS-SLR-VLBI (18); circle, GPS-VLBI (31); triangle, GPS-SLR (20); diamond, SLR-VLBI (4).

Service (IVS) and the International GNSS Service (IGS), respectively. Each set of solutions is composed of intra-technique combined time series of positions and EOPs provided with the full covariance information at each epoch (weekly for SLR and GPS, daily for VLBI). Each solution set has been stacked independently to estimate secular reference frames with consistent EOP time series.

2.1. Input Time Series for ITRF2005

[9] The IGS network comprises 302 sites whose data span 1996.0 to 2006.0. The number of points has increased significantly since 1996.0 to exceed 200 in 2003. The network is almost evenly distributed globally although more stations are located in the Northern Hemisphere. The raw GPS data have been computed by eight analysis centers (ACs), each one providing its solution to the IGS. Weekly combined sets of positions and daily EOPs have been computed from these solutions by the Natural Resources Canada (NRCan) combination center and have been explicitly expressed in ITRF2000 [*Ferland and Hutchison*, 2001; *Ferland*, 2003]. It is worth noting that the IGS weekly solutions have not been homogeneously computed. For example, major changes in the Center for Orbit Determination in Europe (CODE) AC computation strategy have been reported by *Steigenberger et al.* [2006]. As the most recent data have been analyzed with improved modeling, their internal quality is expected to be better.

[10] The ILRS network is composed of 87 stations using data from 1993.0 to 2006.0. Although the ILRS network suffers from an unequally distributed network, the quality of the Lageos 1 and Lageos 2 orbit determination makes this technique essential for the realization of the ITRF origin as the center of mass of the whole Earth system. Its 13-year (a) data span is also essential for ITRF stability monitoring. Weekly sets of positions and daily EOPs have been computed by the Agenzia Spaziale Italiane (ASI) AC within the ILRS Analysis Working Group (AWG) combining data

analyzed by five independent ACs [*Luceri and Pavlis*, 2006]. Although not all the stations observe continuously during the whole week, the ILRS weekly solutions provide station coordinates computed at the mean epoch of each week.

[11] The IVS solutions span 1980.0 to 2006.0 and include 136 radio telescope stations. The number of telescopes per 24-h session varies from 3 to 20. Each session spans a full day but these are not continuous, with an average of about three sessions per week, and the central epochs are at irregular intervals. The combined daily solutions have been computed by the VLBI group at the Geodetic Institute of the University of Bonn from five independent VLBI ACs [*Vennebusch et al.*, 2006]. For this study, we have analyzed only those sessions comprising at least four stations.

[12] ITRF2005 contains 18 sites with colocated VLBI, GPS, and SLR instruments. A map of all colocated sites is shown in Figure 1. There are apparently many colocated sites to study. However, some SLR and VLBI stations have been observed irregularly or for limited periods, and consequently cannot be used to investigate nonlinear behaviors. Only a few colocated sites with sufficient common data spans (out of the entire 10-a overlapping period from 1996.0 to 2006.0) can be used in a quantitative comparison.

[13] All input times series have been computed using a priori models of the reference point motions [*McCarthy and Petit*, 2004]. Solid Earth tides, ocean tide loading as well as pole tide have been modeled in the original data processing. For some of the ACs solutions, pole tide correction has been applied at the intratechnique combination level. However, it is worth noting that atmospheric, hydrological and nontidal ocean loading have not been modeled during AC data processing. As a consequence these geodynamical signals are expected to be contained in the residuals of the first step computation of the ITRF2005. The effect of the VLBI antenna thermal deformation has not been taken into account in the VLBI data processing [*Vennebusch et al.*,

2006]. The use of current thermal deformation model [*McCarthy and Petit*, 2004] has been investigated by [*Tesmer et al.*, 2006]. They have shown that this effect mainly causes annual signal up to 0.7 mm and lead to episodic signal up to ±3 mm in the height component.

2.2. Detrended Height Time Series Computation

[14] IGS, IVS, and ILRS coordinate frame time series have been rigorously stacked using the Combination and Analysis of Terrestrial Reference Frames (CATREF) software [*Altamimi et al.*, 2002] to estimate positions at a reference epoch and velocities for every station. The computation strategy is summarized in this section. For more details about this approach, see *Altamimi et al.* [2006, 2007].

[15] The per technique time series of station positions and EOPs have been combined, rigorously stacked, using the following relation involving the seven Helmert similarity parameters in a Cartesian frame:

$$\forall i, \quad X_k^i(t_k^i) = X_c^i + (t_k^i - t_0)\dot{X}_c^i + T_k + D_k X_c^i + R_k X_c^i \qquad (1)$$

where for each point i of the solution k, $X_k^i(t_k^i)$ is the position (at epoch t_k^i) and X_c^i and $\dot{X}_c^i$ are the position (at the reference epoch t_0) and velocity of the stacked solution c. D_k, T_k and R_k are the scale factor, the translation vector and the rotation matrix, respectively, needed to transform the coordinates of the combined frame at the mean epoch of the solution k into the frame of the individual input set k. T_k contains the three origin components and R_k the three rotations around the three axes X, Y, Z, respectively. Thus seven parameters per input weekly (or session-wise) solution as well as secular coordinates for every station are estimated using the full covariance of every solution to weight the estimation. Frame minimum constraints are added to define the stacked frame and to allow the normal equation inversion [*Altamimi et al.*, 2007].

[16] This approach is used to separate global motion and biases affecting the whole set of stations from the motion of individual stations. Here the motion of each station is modeled as a piecewise linear function so that most of the station nonlinear motion is left in the postfit residuals. A break-wise approach is used to account for discontinuities in the time series due to any physical motion of the ground, such as earthquakes, or equipment changes. Discontinuity files can be found at http://itrf.ensg.ign.fr/. A new stacked station position is estimated after every offset detected. In that case, velocities are usually constrained to be equal before and after a discontinuity, except site where earthquake occurred. A similar velocity constraint is also applied for colocated stations. Noncontinuous preseismic and postseismic deformations have not been modeled in this analysis nor any seasonal term or nonlinear deformation field.

[17] The time series residuals of this computation are assessed in the following. Contrary to the ITRF2005 computation, we reject all VLBI sessions having less than four stations, restricting the number of VLBI sessions to 3259 in the above computation.

2.3. Network Effect

[18] Geodetic position time series contain nonlinear variations which reach several millimeters of amplitude. These are mainly attributed to loading effects which are not modeled at the ACs level (see section 2.1) and to remaining systematic errors. Although equation (1) is weighted by the full covariance matrix of the positions neither time-correlated noise nor nonlinear station motion are modeled. The Helmert parameters of equation (1) are used to compare the piecewise linear positions of the stacked frame to the positions of a frame which undergoes more complex shape deformation. However, theoretically, this relationship can only be rigorously applied when the two frames to be compared have a similar shape. A portion of the station individual motion may consequently leak into the Helmert parameters. As this effect is dependent on the network configuration, we call it "network effect" in the following, as is commonly done. However, it should be noticed that the amplitude of this effect depends additionally on each station individual motion and systematic errors, and on technique internal noise.

[19] The analysis of the network effect needs an a priori knowledge either of the station individual motion or of the transformation parameters. *Blewitt and Lavallée* [2000] have analyzed this effect assuming that loading effects dominate station motions. *Tregoning and van Dam* [2005] have observed that the scale parameter absorbs station motion when transforming station displacements caused by atmospheric loading from a frame centered at the Earth's center of mass (CM) to a frame centered at the Earth's surface barycenter (CF) using a seven-parameter similarity, but their simulation did not model any other systematic errors. *Lavallée et al.* [2006] have also analyzed this effect using synthetic and real data, mentioning that an annual signal in the GPS scale is reduced when the crust deformation field is modeled using loading theory. In the context of ITRF computation, and particularly ITRF2005, the scale has been chosen to be estimated to better monitor any distortion of the weekly (or session-wise) frames. Intrinsic IVS solution scale and ILRS solution translation and scale time series are available from *Altamimi et al.* [2007] (Figures 2 and 3). Their rigorous analysis in the scope of network effect evaluation requires external information such as a loading model, which is beyond the scope of this paper. The analysis of the IGS solution Helmert parameters time series themselves would be useless since IGS weekly frames have already been expressed in ITRF2000: no seasonal pattern is consequently detectable in the IGS solution intrinsic scale time series.

[20] We attempt here to evaluate the network effect using only ITRF2005 data. Our method is to compare station residual time series from different IGS subnetworks stacked to give an order of magnitude of the error introduced by this network effect. The advantage of such an approach is that no assumption about the signal needs to be made neither for the residuals nor for the Helmert parameters. Our experiment, however, only uses an extract of each covariance matrix. The disadvantage is that the covariances involving points which have been removed are neglected. To circumvent this omission and to strictly test the geometrical effect, we have only considered station block diagonal covariance terms in the following either for the subnetwork stacking or for the full IGS network stacking. We first qualify the IGS network and then evaluate the network effects associated with the SLR and VLBI networks.
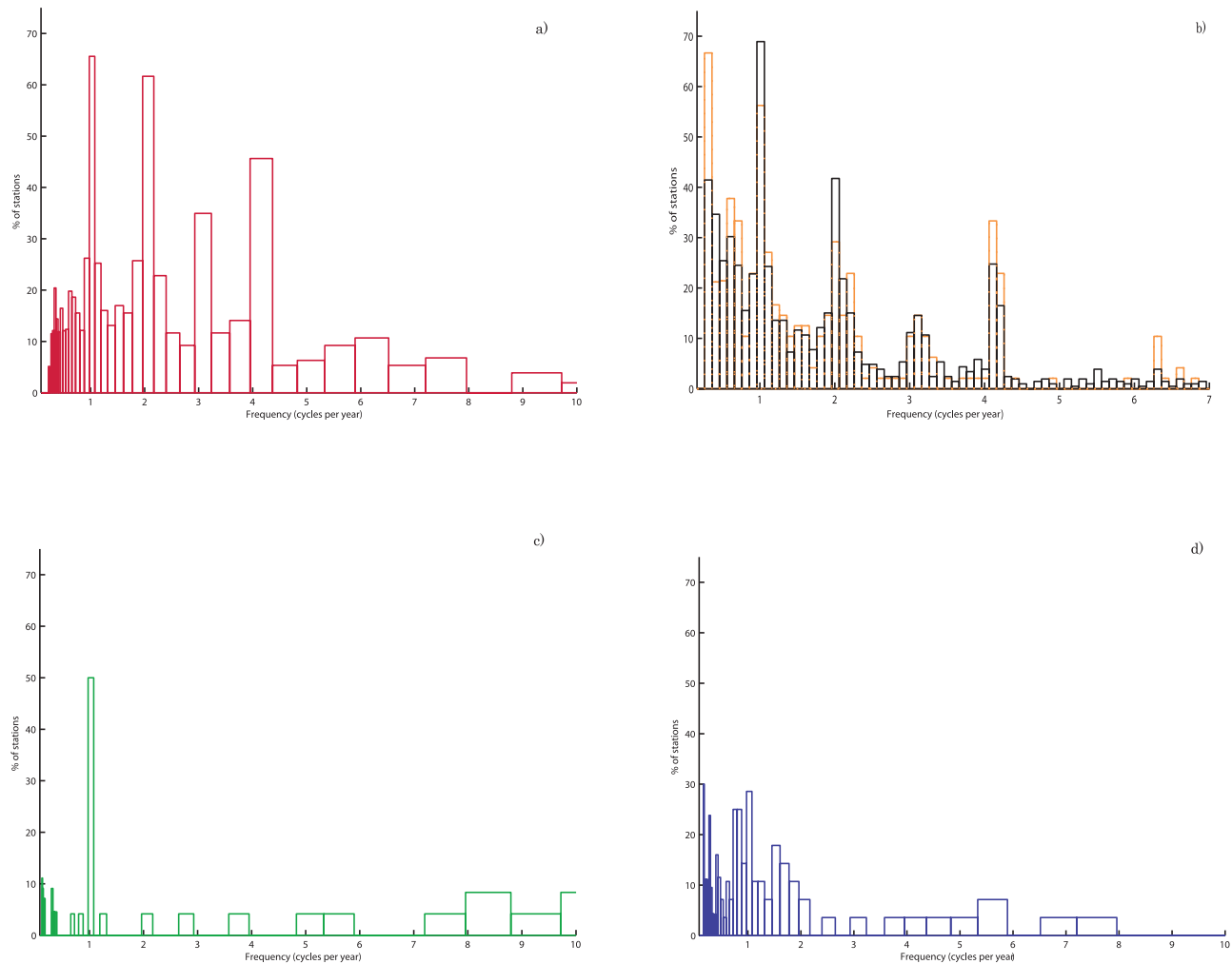
Figure 2. Histograms of the detected frequencies in the ITRF2005 height residuals of the GPS technique with SNR higher than 3.5. (a) With more than 150 points. (b) Detailed histogram with constant bin width. Orange indicates European stations only (48 time series), and black indicates whole set of stations (205 time series) (c) Histogram of the detected frequencies in the ITRF2005 height residuals of the VLBI technique with SNR higher than 3.5. Twenty residual height time series with more than 150 estimated positions are considered. (d) Histogram of the detected frequencies in the ITRF2005 height residuals of the SLR technique with SNR higher than 3.5. 28 residual height time series with more than 150 estimated positions are considered.

[21] The IGS network has a good global coverage but there is a concentration of stations in the Northern Hemisphere and a varying spatial density. As loading effects and/or systematic errors are regionally correlated (due, for example, to similar equipment and monumentation in case of GPS), the aliasing effect is expected to be accentuated. Therefore we have selected a GPS subnetwork which is almost optimal in terms of spatial density. The Earth's surface has been subdivided into 80 faces with almost equal area, based on the first subdivision of an icosahedron centered with respect to the Earth [*Chambodut et al.*, 2005]. Only one IGS station has been chosen per face. The selected network covers 61 faces with, on average, 52% of the stations in the X positive hemisphere, 56% in the Y positive hemisphere and 55% in the Z positive hemisphere (see Table 1). Some of the stations are located in the same site but operate at different epochs. We have also made three

exceptions to the above rule by using stations located close to the boundary of an empty face (MDO1, CRO1 and UNSA). The estimation of the 14-parameter similarity (seven for the positions and seven for their time derivatives) between the stacked frame of this subnetwork and the stacked frame of the full IGS network provides the shape difference between the two solutions. The weighted root mean square scatter (WRMS) of the transformation is 0.4 mm for position and 0.2 mm/a for velocities. The residual time series of the two stackings are almost identical for the horizontal components with scatter of 0.5 ± 0.1 mm. However, a difference of 1.2 ± 0.2 mm is observed for the height component mostly because the two scales differ by an annual term of 1 mm of magnitude. Thus we have observed that the IGS network effect might have an impact of about 1 mm in the heights when changing to a more uniformly distributed network. This analysis implicitly
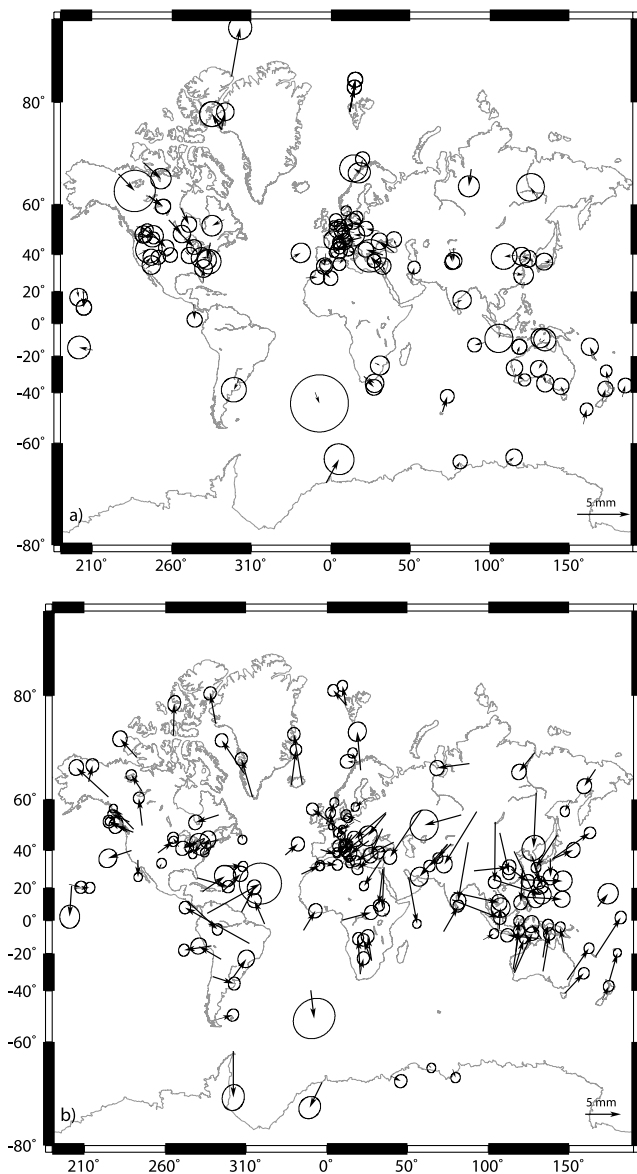
Figure 3. (a) The 4.14 cpy wave estimated in GPS height residual time series having SNRs greater than 3.5. (b) The 1.00 cpy wave estimated in GPS height residual time series having SNRs greater than 3.5. The norm of arrows provides the signal amplitude A and the arrow orientation (counted clockwise from the north) indicates the phase ϕ with respect to the model $A \cos(\omega(t - 2000.0) - \phi)$. The ellipses represent the 95% confidence ellipses.

assumes that a well distributed network does not suffer from network effect, which should not be exactly true because there is no reason that station individual motions cancel each other exactly. With regards to the relatively small value obtained and this consideration we keep IGS network stacking residuals as a reference in the following.

[22] To study VLBI and SLR network effects, IGS colocated subnetworks have been separately extracted from the IGS frames building two subsets of data. These subnetwork frames are then stacked with the same strategy as the

VLBI and SLR input solutions for ITRF2005, using internal constrains to define the combined frames [*Altamimi et al.*, 2007]. On average, 72% of the SLR stations simultaneously operate with a GPS station. As SLR core stations play an important role in the SLR analysis, we paid attention to reject all the weeks where more than two IGS stations colocated with SLR core stations are missing; we assure on average that more than 85% of the SLR core stations are represented in the colocated GPS subset of data. The geometry of the true SLR network is not exactly reproduced in that experiment although the general distribution is quite representative. The stacked solution of this subnetwork is comparable to the full IGS stacked solution. Indeed, a 14-parameter similarity has been estimated between them over stations having more than 150 points. The WRMS agreement of the transformation is at the level of 0.3 mm for positions and 0.1 mm/a for velocities. It is worth noting that there is no significant drift in the translations. The Helmert parameter time series differ from those of the full IGS stacking by 1 mm scatter in each origin component and 2 mm in scale. The two sets of residuals are consequently different. Table 2 shows the computed average scatter between the full GPS residuals and colocated GPS network residuals in the height component. Horizontal components are omitted for clarity but their agreement is at the level of 0.8 ± 0.5 mm, whereas it is 2.1 ± 0.3 mm for the heights in term of scatter.

[23] The same analysis has been conducted for colocated VLBI stations where daily solutions of more than four stations have been used. About 86% of the VLBI stations operate simultaneously with IGS stations. The median number of IVS stations is six per session. As VLBI observes at a daily interval, the GPS subnetwork data of the week has been extracted every time a VLBI session has occurred. Similarly, a 14-parameter similarity has been estimated between the stacked frame of this subnetwork and the full IGS network stacked frame over stations having more than 150 points. The WRMS agreement of the transformation is 1.3 mm for positions and 0.7 mm/a for velocities. Height WRMS values are given in Table 2 for stations having more than 150 points. The horizontal agreement is 1.3 ± 0.5 mm and is 3.0 ± 0.8 mm for the vertical (see Table 2). The level of scatter due to the network effect, as evaluated here, is still lower than the uncertainty of the station positions for SLR and VLBI colocated networks.

[24] As section 4.1 reveals that the annual harmonic is the main common spectral line in the IGS, IVS, and ILRS residuals, we have fitted an annual signal of the residual differences with respect to the full IGS reference residuals for both experiments (see Table 2). The annual signal amplitude is about 1 mm on average for both techniques. There is no significant scale annual signal in the simulated VLBI scale difference with respect to the full IGS scale. We note 0.7 ± 0.1 mm of annual signal in the SLR simulated scale difference. The difference increases at this frequency compared to the well-distributed IGS subnetwork to reach 0.9 ± 0.1 mm and 1.4 ± 0.2 mm for VLBI and SLR, respectively, with consistent phases for the two signals. It seems consequently that the scale affects the three techniques quite similarly at the annual frequency, mainly due the asymmetry between the Northern and Southern Hemi-

Table 1. IGS Station Subnetwork Selected to Constitute a Spatially Well-Distributed Network

Code	N[a]	Long, deg	Lat, deg	WRMS E, mm	WRMS N, mm	WRMS U, mm	$t_{start} - t_{end}$[b]	Code	N	Long, deg	Lat, deg	WRMS E, mm	WRMS N, mm	WRMS U, mm	$t_{start} - t_{end}$[b]
ALIC	382	133.9	−23.5	1.6	1.3	5.4	1998.5−2006.0	LHAS	417	91.1	29.5	2.2	2.5	7.2	1996.8−2006.0
AOML	308	−80.2	25.6	2.1	1.6	5.6	1998.2−2004.3	MALI	492	40.2	−3.0	3.3	2.2	7.2	1996.1−2006.0
ASC1	404	−14.4	−7.9	2.7	1.7	5.8	1996.3−2005.6	MAS1	493	−15.6	27.6	1.7	1.9	5.2	1996.1−2006.0
ASPA	151	−170.7	−14.2	3.0	1.6	6.8	2003.1−2006.0	MCM4	501	166.7	−77.8	2.4	1.7	8.4	1996.1−2006.0
AUCK	506	174.8	−36.4	3.4	1.6	4.6	1996.1−2006.0	MDO1	515	−104.0	30.5	1.8	1.7	4.6	1996.1−2006.0
BAHR	472	50.6	26.1	2.0	2.1	6.0	1996.6−2006.0	MSKU	93	13.6	−1.6	2.5	1.7	4.9	2001.4−2005.3
BAKO	319	106.9	−6.5	2.0	2.1	7.3	1998.3−2006.0	NKLG	288	9.7	0.4	1.8	1.5	5.5	2000.3−2006.0
BILI	268	166.4	67.9	1.3	2.0	5.3	1999.7−2006.0	NLIB	516	−91.6	41.6	1.8	1.8	5.3	1996.1−2006.0
BRAZ	277	−47.9	−15.9	2.0	1.5	8.3	1996.7−2006.0	NOUM	392	166.4	−22.1	3.6	1.8	6.5	1998.2−2006.0
BRUS	513	4.4	50.6	1.7	1.6	3.4	1996.1−2006.0	NTUS	347	103.7	1.3	2.0	2.2	5.6	1997.7−2006.0
CHAT	507	−176.6	−43.8	2.8	1.8	4.7	1996.1−2006.0	NYAL	487	11.9	78.9	1.5	1.8	5.6	1996.1−2006.0
COCO	470	96.8	−12.1	1.9	1.9	4.6	1996.5−2006.0	OHI3	115	−57.9	−63.2	2.0	2.5	6.3	2003.5−2005.9
CRO1	479	−64.6	17.7	2.7	1.9	7.0	1996.1−2006.0	OHIG	199	−57.9	−63.2	2.8	3.1	8.7	1996.1−2002.1
DAV1	474	78.0	−68.5	1.8	1.7	4.4	1996.1−2006.0	ONSA	509	11.9	57.2	1.3	1.1	3.2	1996.1−2006.0
DGAR	370	72.4	−7.2	2.4	2.2	5.1	1996.4−2006.0	PETP	373	158.6	52.9	1.9	1.8	5.6	1998.8−2006.0
DRAO	518	−119.6	49.1	1.9	1.8	4.8	1996.1−2006.0	POL2	450	74.7	42.5	1.7	1.6	4.7	1996.1−2006.0
EISL	354	−109.4	−27.0	4.2	2.0	7.4	1996.1−2003.8	QAQ1	178	−46.1	60.6	0.9	1.2	5.1	2002.5−2006.0
FORT	500	−38.4	−3.9	3.1	2.3	6.6	1996.1−2006.0	RAMO	348	34.8	30.4	3.1	1.9	5.6	1998.5−2006.0
GALA	205	−90.3	−0.7	2.1	1.6	4.7	1996.7−2002.9	REYK	507	−22.0	64.0	2.3	1.6	6.3	1996.1−2006.0
GLPS	130	−90.3	−0.7	1.3	1.9	3.7	2003.3−2006.0	RIOG	429	−67.8	−53.6	1.5	2.2	5.2	1997.7−2006.0
GOLD	518	−116.9	35.2	2.0	2.5	4.5	1996.1−2006.0	SANT	505	−70.7	−33.0	2.1	2.3	6.1	1996.1−2006.0
GOUG	249	−9.9	−40.2	3.1	2.1	13.7	1998.7−2006.0	SEY1	145	55.5	−4.6	2.9	2.3	6.5	1999.2−2005.2
GUAM	497	144.9	13.5	2.7	2.2	5.3	1996.1−2006.0	STJO	516	−52.7	47.4	1.7	1.4	4.2	1996.1−2006.0
HOB2	475	147.4	−42.6	2.2	1.5	5.5	1996.2−2006.0	SUTH	361	20.8	−32.2	2.7	1.5	4.7	1998.3−2006.0
HRAO	414	27.7	−25.7	2.0	1.9	5.3	1996.8−2006.0	THTI	355	−149.6	−17.5	2.9	1.9	5.9	1998.5−2006.0
IISC	421	77.6	12.9	2.2	1.5	7.1	1997.4−2006.0	TIXI	369	128.9	71.5	1.7	2.3	6.4	1998.8−2006.0
INVK	211	−133.5	68.1	1.7	2.3	8.9	2001.9−2006.0	TOW2	384	147.1	−19.2	2.0	1.6	4.6	1998.5−2006.0
IRKT	495	104.3	52.0	2.0	2.2	8.1	1996.1−2006.0	TSKB	504	140.1	35.9	2.3	2.4	6.8	1996.1−2006.0
ISPA	84	−109.3	−27.0	1.8	1.2	5.9	2004.2−2006.0	UNSA	271	−65.4	−24.6	1.8	1.6	6.0	2000.3−2006.0
KERG	488	70.3	−49.2	2.0	2.2	4.3	1996.1−2006.0	VESL	257	−2.8	−71.6	1.7	1.7	7.3	1998.8−2006.0
KIT3	392	66.9	39.0	2.1	2.6	5.0	1996.1−2006.0	VILL	500	−4.0	40.3	1.5	1.4	3.7	1996.1−2006.0
KOKB	495	−159.7	22.0	2.8	1.8	5.5	1996.6−2006.0	WUHN	484	114.4	30.4	2.3	1.9	6.5	1996.6−2006.0
KOUR	482	−52.8	5.2	2.4	2.6	6.7	1996.1−2006.0	YAR2	501	115.4	−28.9	2.3	1.9	6.3	1996.1−2006.0
KWJ1	277	167.7	8.7	3.1	2.3	6.9	1996.2−2002.6								

[a]Number of weekly estimated positions available over the interval 1996.0−2006.0.
[b]Data span of the station.

sphere. The effect of these added annual terms may be a reduction or an amplification of the real measured annual displacement. The phase may shift, but this shift may be reasonably small if the station displacement is much larger than the added annual error.

[25] This experiment provides an indication of the geometrical effect caused by the stacking strategy but does not constitute an exact answer. Indeed, the SLR and VLBI techniques are not subject to the same systematic errors as GPS is and do not provide the same level of measurement noise. Thus, although our experiment quite faithfully reproduces the geometry of the networks, it does not reproduce the exact station position measurement as viewed by the SLR or VLBI techniques. It is, however, reasonable to take the values of 2 mm and 3 mm as measurement of the network effect for SLR and VLBI, respectively.

3. Height Residual Analysis

[26] Before entering into more details, it is worth briefly discussing the scatter of the position residual time series. IGS position residual WRMS is typically at the level of 1.8 mm for both horizontal components and 5.3 mm for heights. IVS position residuals have scatter of 3.5 mm and 4.4 mm,

respectively, and ILRS residuals have nearly equal scatter in all components with 8.7 mm horizontally and 8.5 mm vertically for the core stations. *Ray et al.* [2007] have also analyzed the spectral content of the ITRF2005 ILRS, IVS, and IGS position residuals by stacking the normalized periodograms. They conclude that GPS residuals on the three components are dominated by flicker noise and that IVS and ILRS power spectra are much whiter. This work uses the same data set, except that we restrict here the number of VLBI sessions used. However, this work is devoted to individual station residual analysis. The vertical component is more interesting to study since loading signals are larger than for the other components [*Farrell*, 1972]. Systematic errors are expected to be more important too in that component due mainly to the geometry of the measurements, troposphere refraction and data analysis. The scattering of SLR residuals on the horizontal component also decreases the interest of intercomparing horizontal residuals since only GPS and VLBI techniques would be worth comparing, restricting the analysis to two independent data sets only. We consequently limit this analysis to the vertical component but the horizontal component issue is addressed if it clarifies or enriches the discussion. The reader may refer

Table 2. WRMS and Amplitude and Phase of the Annual Term Computed Over the Differences Between the Residuals Produced With the Subnetwork Stacking and the Residuals of the Full IGS Network Stacking[a]

DOMES	Code	$WRMS_{Up}$, mm	$\bar{\sigma}_{Up}$,[b] mm	A, mm	ϕ, deg	Number of Points
GPS Network Colocated With SLR Network						
42202M005	AREQ	2.9	8.6	1.7 ± 0.4	15 ± 10	164
12205M002	BOR1	2.0	6.0	1.5 ± 0.2	35 ± 7	256
40451M123	GODE	2.0	6.8	0.3 ± 0.1	22 ± 21	373
10002M006	GRAS	2.1	7.7	1.1 ± 0.1	152 ± 8	294
11001M002	GRAZ	2.0	5.9	0.5 ± 0.1	65 ± 15	377
13212M007	HERS	1.8	5.6	0.6 ± 0.2	325 ± 13	252
30302M004	HRAO	1.9	5.3	0.9 ± 0.2	80 ± 14	164
12734M008	MATE	2.2	5.5	0.7 ± 0.2	320 ± 16	261
40442M012	MDO1	2.1	7.7	0.5 ± 0.1	35 ± 15	377
40497M004	MONP	2.8	11.7	0.4 ± 0.2	354 ± 22	352
14106M003	POTS	2.0	4.7	1.2 ± 0.1	66 ± 7	319
13402M004	SFER	2.1	5.8	0.6 ± 0.1	331 ± 17	190
21605M002	SHAO	2.4	9.7	0.3 ± 0.3	152 ± 60	147
14201M010	WTZR	1.9	3.7	1.1 ± 0.1	40 ± 7	332
50107M004	YAR2	2.7	5.6	1.1 ± 0.1	138 ± 9	388
14001M004	ZIMM	2.2	6.0	1.0 ± 0.2	81 ± 10	268
GPS Network Colocated With VLBI Network						
40104M002	ALGO	2.4	3.5	1.0 ± 0.1	41 ± 7	465
41719M002	CONZ	2.8	6.2	0.9 ± 0.2	270 ± 14	248
40408M001	FAIR	4.4	5.0	0.3 ± 0.2	184 ± 33	790
41602M001	FORT	3.8	9.8	0.8 ± 0.2	119 ± 14	520
50116M004	HOB2	4.5	4.7	2.2 ± 0.3	228 ± 9	171
30302M004	HRAO	4.1	6.0	0.9 ± 0.3	160 ± 17	324
40424M004	KOKB	4.5	5.3	0.6 ± 0.2	49 ± 18	703
12734M008	MATE	3.2	4.8	0.6 ± 0.2	140 ± 22	311
12711M003	MEDI	2.4	6.9	0.5 ± 0.3	335 ± 26	149
10317M001	NYAL	3.5	7.5	1.1 ± 0.2	61 ± 11	557
10402M004	ONSA	2.3	3.9	0.6 ± 0.2	333 ± 19	184
21730S005	TSKB	2.6	4.3	2.1 ± 0.3	217 ± 7	179
40440S020	WES2	2.6	6.1	0.6 ± 0.1	122 ± 16	481
14201M010	WTZR	2.4	3.6	0.6 ± 0.1	55 ± 10	872

[a]Amplitudes and phases are provided with respect to the model $A \cos(\omega(t - 2000.0) - \phi)$.

[b]Median value of the height residual error bars.

to *Ray et al.* [2007] for more insights on the horizontal component power spectra.

[27] In the ideal world, we would expect the three techniques height measurements to represent the physical motion of the Earth's crust. They are expected to contain a common spectral signature which represents the local ground motion. The reality may be much more complicated because each technique could be subject to its own peculiar systematic errors, such as signal multipath for GPS, or because of technique own aliasing. Indeed, ground motions that are not modeled at the raw geodetic data analyses (ACs) level may cause artificial spectral lines or complex noise processes at the geophysical frequencies of interest and may be misinterpreted as physical ground motion [*Stewart et al.*, 2005]. Discrepancies among techniques may consequently be found in the derived height residuals.

[28] This section presents the spectral method used to analyze the time series. It comes with a description of the method developed to compute a correlation coefficient between two independent height time series.

3.1. Spectral Analyses Using Frequency Mapping

[29] In general, the height residual time series are unevenly sampled. In space geodesy literature, spectral analysis of such data are often conducted using a Lomb periodogram [*Scargle*, 1982] or similar method [*Langbein and Johnson*, 1997; *Titov and Yakovleva*, 1999; *Mao et al.*, 1999; *Blewitt and Lavallée*, 2002]. According to *Scargle* [1982], this algorithm is equivalent to the fitting of sine waves directly to the data. Interpreting such periodograms when dealing with irregular samples requires caution since the observing window contributes to the spectrum. This contribution is sensitive to the real spectral content of the data so that artificial spikes may be created if sampling is uneven.

[30] The Frequency Analysis Mapping on Unusual Sampling (FAMOUS) software is specifically designed to search for sets of frequencies in discrete irregular sampled data sets [*Mignard*, 2005]. The algorithm builds a least squares periodogram to detect the most powerful spectral line and uses a nonlinear least squares fit to improve the frequency location. Once a spectral line has been estimated, it is removed from the data set and the periodogram of the residuals is computed to detect the next most significant spectral line. At each step, all frequencies, as well as the trend, are readjusted in a nonlinear optimization adjustment. Finally, frequencies are filtered by means of a signal-to-noise ratio test to keep only the significant spectral lines. The significance of the detected spectral lines is assessed in the spectral domain by dividing the square root of the power of the line by a robust estimation of the noise computed once the line is removed. For more details about the algorithm, see *Mignard* [2005]. The GPS power spectrum is known to contain correlated noise (see section 4.1 for references). We choose anyway to test the significance of the lines assuming background white noise in order to analyze the low-frequency signal.

[31] Moreover, the height residual time series we aim to analyze contain points with heterogeneous quality. This heterogeneity is expected to be reflected in the position formal errors supplied with the solutions. An analysis of these uncertainties exhibits nonnegligible heterogeneities in the VLBI and SLR height determinations especially, as well as in the early GPS data. However, GPS uncertainties are more stable even if some seasonal variations of minor amplitudes, mostly semiannual, are found in most of the site formal error time series.

[32] It is necessary to take into account these uncertainties in the spectral analysis. The use of the inverse of the square of these quantities is the optimal weight to consider in estimations. So adjustments of periodograms and nonlinear optimizations need to be weighted in the FAMOUS algorithm to compute more reliable estimates of spectral lines in the height time series. We have consequently added this feature to the software.

3.2. Correlation Study

[33] We aim to compare height time series from different techniques and to assess their possible agreement. Computing a correlation coefficient is not easy because of data gaps and sampling discrepancies. GPS and SLR point positions and VLBI point positions do not reflect the same physical

quantity: GPS and SLR positions are weekly integrations of mean motion whereas VLBI positions are daily integrations. Averaging VLBI data at the GPS or SLR sampling would not be reasonable because of VLBI data sparseness. We have adopted a time evolution model of the data to deal with data gaps and this heterogeneous sampling. In doing so, we add stochastic information to model the time evolution of the data. The GPS and SLR averaging process of daily positions also need to be modeled in the comparison method.

3.2.1. Correlation Computation Equations

[34] Our method is based on a nonadaptative Kalman filter: a complete review of Kalman filtering and basic random processes is given, for example, by *Herring et al.* [1990]. The state-space model used in the Kalman filter formalism is particularly adapted to describe the time evolution of a random process. The random process, called the state, does not necessarily need to be directly observable: the observations, here a pair of height residuals from two distinct techniques, can be related to the random process as a linear combination, plus an additive noise. We present the model used to compare weekly time series to daily time series, for example, GPS or SLR residual height time series and VLBI residual height time series. In our case, we would like to estimate the daily height motion viewed by the two techniques. In the following, we call this daily height the state height. Thus our state vector contains at least two parameters, one for the state height as viewed by each technique. However, GPS and SLR height residuals represent a weekly mean height with an average of seven consecutive daily height parameters. Seven state parameters are then needed for GPS or SLR vectors and one state parameter is needed for each VLBI state height which is directly observable.

[35] The dynamics of the state parameters are given in the Kalman filter state equation. Two consecutive positions z_{t+1} and z_t are modeled to differ by a white noise contribution, the innovations V_t:

$$Z_{t+1} = A_t Z_t + V_t$$

$$
\begin{bmatrix}
z^{vlbi}_{(t+4)} \\
z^{gps}_{(t-2)} \\
z^{gps}_{(t-1)} \\
z^{gps}_{(t)} \\
z^{gps}_{(t+1)} \\
z^{gps}_{(t+2)} \\
z^{gps}_{(t+3)} \\
z^{gps}_{(t+4)}
\end{bmatrix}
=
\begin{bmatrix}
1 & 0 & 0 & 0 & 0 & 0 & 0 & 0 \\
0 & 0 & 1 & 0 & 0 & 0 & 0 & 0 \\
0 & 0 & 0 & 1 & 0 & 0 & 0 & 0 \\
0 & 0 & 0 & 0 & 1 & 0 & 0 & 0 \\
0 & 0 & 0 & 0 & 0 & 1 & 0 & 0 \\
0 & 0 & 0 & 0 & 0 & 0 & 1 & 0 \\
0 & 0 & 0 & 0 & 0 & 0 & 0 & 1 \\
0 & 0 & 0 & 0 & 0 & 0 & 0 & 1
\end{bmatrix}
\begin{bmatrix}
z^{vlbi}_{(t+3)} \\
z^{gps}_{(t-3)} \\
z^{gps}_{(t-2)} \\
z^{gps}_{(t-1)} \\
z^{gps}_{(t)} \\
z^{gps}_{(t+1)} \\
z^{gps}_{(t+2)} \\
z^{gps}_{(t+3)}
\end{bmatrix}
+
\begin{bmatrix}
v^{vlbi}_{(t+3)} \\
0 \\
0 \\
0 \\
0 \\
0 \\
0 \\
v^{gps}_{(t+3)}
\end{bmatrix}
$$

$$(2)$$

where $z^{vlbi}_{(t)}$, $z^{gps}_{(t)}$ are the state daily heights viewed by VLBI and GPS, respectively, at the epoch t. The innovations, $v^{vlbi}_{(t)}$ and $v^{gps}_{(t)}$, may be different for each technique but are assumed to be correlated. This correlation is modeled in the

innovation vector $V(t)$ variance-covariance matrix, assumed to be

$$
\text{Var}(V_t) =
\begin{bmatrix}
\sigma^2_{wnvlbi} & 0 & \cdots & \cdots & 0 & \rho\sigma_{wnvlbi}\sigma_{wngps} \\
0 & 0 & & & & 0 \\
\vdots & & \ddots & & & \vdots \\
\vdots & & & \ddots & & \vdots \\
0 & & & & 0 & 0 \\
\rho\sigma_{wnvlbi}\sigma_{wngps} & 0 & \cdots & \cdots & 0 & \sigma^2_{wngps}
\end{bmatrix}
$$

$$(3)$$

The correlation coefficient ρ and the white noise variances σ^2_{wnvlbi} and σ^2_{wngps} are unknown and are our parameters of interest.

[36] Our sampling problem is solved in the measurement equation of the Kalman filter. When GPS and VLBI data are available at 3-d intervals, our observation equation is written as

$$
\begin{bmatrix}
h^{vlbi}_{(t+3)} \\
h^{gps}_{(t)}
\end{bmatrix}
=
\begin{bmatrix}
1 & 0 & 0 & 0 & 0 & 0 & 0 & 0 \\
0 & \frac{1}{7} & \frac{1}{7} & \frac{1}{7} & \frac{1}{7} & \frac{1}{7} & \frac{1}{7} & \frac{1}{7}
\end{bmatrix}
\begin{bmatrix}
z^{vlbi}_{(t+3)} \\
z^{gps}_{(t-3)} \\
z^{gps}_{(t-2)} \\
z^{gps}_{(t-1)} \\
z^{gps}_{(t)} \\
z^{gps}_{(t+1)} \\
z^{gps}_{(t+2)} \\
z^{gps}_{(t+3)}
\end{bmatrix}
+
\begin{bmatrix}
u^{vlbi}_{(t+3)} \\
u^{gps}_{(t)}
\end{bmatrix}
$$

$$H_t = C_t Z_t + U_t \qquad (4)$$

where $h^{vlbi}_{(t)}$ and $h^{gps}_{(t)}$ are the height residuals at the epoch t. In equation (4), we assume that the VLBI measurement is an observation of the daily position which is a first approximation because the middle of the session does not coincide with the middle of the day. The random process U_t models the measurement noise which is assumed to be uncorrelated. The covariance matrix of the measurement noise is

$$
\text{Var}(U_t) =
\begin{bmatrix}
\boldsymbol{\sigma_{0vlbi}}^2 \sigma^2_{vlbi_{obs}(t+3)} & 0 \\
0 & \boldsymbol{\sigma_{0gps}}^2 \sigma^2_{gps_{obs}(t)}
\end{bmatrix}
\qquad (5)
$$

[37] An indication of the measurement noise is provided with the height residuals through the covariance matrix of the associated observations where $\sigma^2_{gps_{obs}}$ and $\sigma^2_{vlbi_{obs}}$ are taken from. Our combination experiment encourages us to rescale these quantities, which are overly optimistic. This is done through the variance factor parameters σ^2_{0gps} and σ^2_{0vlbi}. When one of the two observations is not available, the corresponding line of this equation is removed.

[38] Equations (2) and (4) are used to estimate the state vector and its covariance matrix at daily sampling from the first day to the last day of common observation span, by using the Kalman filter equations [*Herring et al.*, 1990]. However, the matrices of this model are dependent on some

Table 3. Results of the Tests of the ML Estimator on Synthetic GPS and VLBI Time Series[a]

	σ_{VLBI}, mm d$^{1/2}$	σ_{GPS}, mm d$^{1/2}$	ρ	σ^0_{VLBI}	σ^0_{GPS}
Simulated parameters	0.600	0.600	0.300	1.000	1.000
Mean of estimated parameters	0.596	0.597	0.306	0.999	0.999
Square root of mean variances	0.064	0.072	0.148	0.055	0.042
Square root of the MSE	0.067	0.074	0.146	0.055	0.042

[a]There are 350 points per technique; 1000 simulations. The parameters used to generate these simulated data are listed as well as the average estimates and the mean square error (MSE).

parameters which are the following: the innovations variances σ^2_{wngps} and σ^2_{wnvlbi} and their correlation ρ and scaling factors σ^2_{0vlbi} and σ^2_{0gps}. These five parameters are estimated by maximum likelihood (ML).

[39] The log likelihood of the observation vector H_t is built according to *Gourieroux and Monfort* [1997] under Gaussian assumption by

$$\log(L_H)(H_t; \underline{\theta}) = -\frac{1}{2} \sum_{t=1}^{n} \left\{ \log\left[\det\left[\text{Var}\left(\hat{H}_{t+1|t}\right)(\underline{\theta})\right]\right] \right\}$$
$$-\frac{1}{2} \sum_{t=1}^{n} \left[\dim(H_t) \log(2\pi)\right]$$
$$-\frac{1}{2} \sum_{t=1}^{n} \left(H_t - \hat{H}_{t+1|t}(\underline{\theta})\right)^T$$
$$\cdot \text{Var}\left(\hat{H}_{t+1|t}(\underline{\theta})\right)^{-1}\left(H_t - \hat{H}_{t+1|t}(\underline{\theta})\right) \quad (6)$$

where $\hat{H}_{t+1|t}$ and $var(\hat{H}_{t+1|t})$ are the prediction of the observation at time $t + 1$ and its covariance matrix built using the whole set of observations before time t, respectively. These quantities are computed using the estimates of the Kalman filter and their covariance matrices [*Gourieroux and Monfort*, 1997]. According to equation (6), the Kalman filter needs to be run fully forward to evaluate the log likelihood. This log likelihood is minimized using the downhill simplex method [*Press et al.*, 1996].

[40] The Kalman filter model is slightly modified to estimate the correlation coefficient between SLR and GPS data. We assume the SLR positions to be mean motions over an entire week although this is not strictly true. Indeed, the SLR network only tracks satellites when they are observable and when weather conditions allow. The same can also be said for GPS where observations for an entire week are not always used for every station. However, the information of the midpoint epoch of the observations is stored in the IGS solution files. We consider this epoch to be the epoch of a weekly position because the information of the exact integration time is not always directly available. With

respect to these concerns, the sample epochs are not equal. The previous model has to be modified to use 14 state model parameters to represent the averaging process in the observation equation. Observations at the same epoch can be used when they are both available, equation (4) becomes

$$\begin{bmatrix} h^{slr}_{(t)} \\ h^{gps}_{(t)} \end{bmatrix} = \begin{bmatrix} \frac{1}{7}I_7 & 0 \\ 0 & \frac{1}{7}I_7 \end{bmatrix} \begin{bmatrix} z^{slr}_{(t-3)} \\ \vdots \\ z^{slr}_{(t+3)} \\ z^{gps}_{(t-3)} \\ \vdots \\ z^{gps}_{(t+3)} \end{bmatrix} + \begin{bmatrix} u^{slr}_{(t)} \\ u^{gps}_{(t)} \end{bmatrix} \quad (7)$$

where I_7 is the identity matrix.

3.2.2. Estimator of the Parameter Variances

[41] In the case of an asymptotic normal distribution for the ML estimator, the covariance matrix of the parameters can be estimated analytically. It is the opposite of the inverse of the Hessian matrix of the log likelihood function computed at the point of the maximum. For example, this estimator has been used by *Zhang et al.* [1997] to estimate the variance of their ML estimator of the random walk and white noise variances which were assumed to model the noise in GPS position time series. Conversely, *Langbein and Johnson* [1997] have proposed a method which relies on a Montè Carlo simulation to compute error bars. In the following, we check if the Hessian matrix can be used to compute the estimate covariance matrix in our specific application.

[42] To do so, simulated data must first be generated and used as input to our estimator to compute a scatter of the estimated parameters around the simulated values. Empirical mean square errors (MSE) are compared to the second derivative mean values in Tables 3 and 4 for 1000 simulations of 350 points without gaps. The variance estimates provide similar results. When comparing VLBI and GPS the innovation variance of VLBI is better determined than in GPS because the VLBI daily motion is directly observed. Conversely, the variance factor of GPS measurement noise is better determined. Indeed, it is easier to distinguish the measurement noise from the state dynamics, which are averaged in the case of the GPS model.

[43] As the MSE computation is time consuming, the second derivative evaluation to compute uncertainties for estimated parameters is retained.

4. Results

4.1. Spectral Content

[44] All stations having more than 150 estimated positions are analyzed to search for up to 10 significant frequencies, each with signal-to-noise ratio (SNR) higher

Table 4. Results of the Tests of the ML Estimator on Synthetic GPS and SLR Time Series[a]

	σ_{SLR}, mm d$^{1/2}$	σ_{GPS}, mm d$^{1/2}$	ρ	σ_{SLR}^0	σ_{GPS}^0
Simulated parameters	0.600	0.600	0.300	1.000	1.000
Mean of estimated parameters	0.597	0.595	0.289	0.999	1.001
Square root of mean variances	0.073	0.073	0.156	0.042	0.042
Square root of the MSE	0.072	0.073	0.157	0.042	0.043

[a]There are 350 points per technique; 1000 simulations.

than 3.5. As the frequencies are estimated in a nonlinear least squares adjustment, the uncertainties on the frequency locations can be computed as well as the uncertainties for the amplitudes and phases. The precision of the frequency location is mainly related to the presence of noise in the data and to the number of data samples. Assuming normal background decorrelated noise and given our data span, we estimate the precision of the annual frequency location to be on the order of 10^{-2} cpy for SLR data and better than 10^{-2} cpy for VLBI and GPS. The width of the detected spectral lines in the frequency domain cannot be thinner than 0.106, 0.092, and 0.052 cpy for GPS, SLR, and VLBI, respectively, which give an order of magnitude of the maximum spectral resolution.

[45] The assessment of the detected frequencies is presented as histograms of the proportion of stations for which detected frequencies in a given frequency bin exist. The spectral bins are chosen to be constant in the logarithmic scale such that the logarithm of the ratio of two consecutive bin frequencies is equal to 0.1 (see Figures 2a, 2c, and 2d). It should be noted that only stations providing data lengths longer than 2 times the period of the spectral line are counted in the bins of these histograms.

[46] The GPS power spectrum has already been extensively analyzed during the last decade. It contains a flicker noise background spectrum and white noise [Zhang et al., 1997; Mao et al., 1999; Williams et al., 2004; Le Bail et al., 2007]. Annual and semiannual frequencies have also been widely detected [Mao et al., 1999; Blewitt and Lavallée, 2000; Dong et al., 2002]. Blewitt and Lavallée [2002] have also reported other annual frequency harmonics. Using ITRF2005 IGS residuals, Ray et al. [2007] have investigated these harmonics accurately. They have shown that these frequencies were not exactly located at integer values either on vertical or horizontal components. A model of harmonics of the 1.04 cpy frequency fits their locations very well. The authors have suggested that these could be systematic errors related to the GPS satellite orbits combined with the geometry of the measurements. Figure 2a shows the results of our study. The proportion of significant spectral lines in every frequency band with SNR higher than 3.5 is presented. This analysis reveals that 71% of GPS station height residual time series have a significant signal at a frequency located between 0.95−1.05 cpy with SNR higher than 3.5. This annual frequency comes with a semiannual frequency, and frequencies at the previously mentioned harmonics. This study gives median frequencies of 3.09 cpy and 4.14 cycles per year with scatters of 0.09 cpy for these two frequencies (see Figure 2b). These are consistent with the values 3.12 and 4.16 cpy suggested by Ray et al. [2007]. It confirms that these harmonics are detectable in the individual time series. The annual and semiannual as well as 3.09 and 4.14 cpy signals have been estimated for every height time series with a significant spectral line detected around 4.14 cpy. Figure 3a shows the distribution of the 4.14 cpy spectral line using the convention of Dong et al. [2002] for the representation: the norms of the vectors indicate the signal amplitudes whereas their orientations give the phases. For most stations, the amplitude of the signal is less than 2 mm for these two frequencies. The stations having the most powerful signals at 4.14 cpy are located at high latitude and notably in North America. The

amplitude reaches 4.6 ± 0.5 mm at the GPS Alert station in northeastern Canada with SNR up to 10. Moreover, it is noteworthy that some areas of the world like North America, western Europe and the Persian Gulf exhibit a clear spatial correlation of this signal. These harmonics are also detectable in the horizontal position time series with less than half a millimeter of amplitude on average.

[47] The VLBI histogram in Figure 2c has been built with 20 stations. The ITRF2005 VLBI residual height time series contain mainly white noise [Ray et al., 2007], but with higher level than GPS. As a consequence, the SNR is much lower than for GPS. Only the annual frequency seems to be largely detected in the analyzed set. We can also notice a few low frequencies, but it represents one or two stations in each lower bin. Half of the analyzed time series have significant power (SNR >3.5) between 0.95−1.05 cpy. Some few frequencies have been detected at higher location, but we interpret them as noise. No other frequency than the annual has been largely detected in the horizontal component as well. We notice that the semiannual signature reported by Titov and Yakovleva [1999] and Petrov and Ma [2003] has not been detected here. Tesmer et al. [2007] have, however, reported a semiannual signal in the VLBI scale as well as annual. This signal has been shown to be robust whatever the mapping function used to model the tropospheric delay. We detect annual and semiannual signals as well in the IVS solution scale at the level of 2.9 ± 0.1 mm and 1.2 ± 0.1 mm, respectively, for these two frequencies. We have computed these values using data after 1993.0 because the number of stations has increased since that time [Tesmer et al., 2007]. Moreover, we think that the network effect could add noise processes which generally decrease the signal-to-noise ratio of the underlying signals.

[48] The SLR power spectrum is more evenly dispersed. Figure 2d has been obtained by analyzing 28 position time series. There are several frequency intervals containing significant spectral lines. The annual frequency is detected in 8 time series in the interval 0.95−1.05 cpy. Semiannual signals are detected in Riyadh, Arequipa, and Quincy time series. Riyadh station is not collocated, and the last two time series are not consistent with the colocated GPS data. We detect other groups of frequencies for some stations. There is a wide range of frequencies detected between 0.75 and 0.9 cpy, as well as some lower frequencies. The horizontal power spectra contain, however, few significant spectral lines as well, except the annual signature and some isolated groups of frequencies representing few stations. There is therefore no global signature at fixed frequencies in the ILRS residuals.

[49] The GPS power spectrum contains important power at low frequency. In fact, the power spectrum characteristics depend on the area of the world. For example, Figure 2b shows frequencies distribution in the global spectrum over Europe compared to the full network. The 6th anomalous harmonic is detectable in this area for a few stations. European stations also contain more power between 0.33 and 0.36 cpy. A fit at 0.35 cpy in the height residuals time series having more than 400 estimated positions reveals in phase signal over central Europe up to 2 mm. This result reveals possible spatially correlated low-frequency signals in the GPS data. This type of signal is usually analyzed as

being part of a flicker noise background spectrum and is analyzed in term of variance level. Such analysis shows that the phase is worth studying. Nevertheless, such results need to be analyzed with caution because IGS data have not been computed homogeneously over time. Such low-frequency signals would be worth studying with reprocessed GPS time series such as the ones computed at the Technical Universities of Munich and Dresden [*Steigenberger et al.*, 2006].

4.2. Annual Spectral Line

[50] The annual signal of ITRF2005 height residuals is carefully studied as it is the only common spectral feature of the three observing techniques. An annual signal, as well as a constant, have been fitted by weighted least squares for each colocated site height residual time series with more than 150 points and for all GPS stations with a significant annual frequency (SNR >3.5). We consequently assume here that the annual amplitude of the signal, as well as its phase are constant with time. A semiannual signal has been fitted simultaneously for GPS stations. The order of magnitude of the GPS annual amplitudes is less than 1 cm, the maximum being found at the Brazilia GPS station (BRAZ). The median value lies around 3–4 mm. Figure 3b shows the distribution of the estimated annual GPS signals using the conventions of *Dong et al.* [2002] for the representation. Thus a vector pointing directly north describes an annual motion having a maximum in January or a vector pointing east describes an annual motion with its maximum in April. Figure 3b shows all stations having a significant annual signal detected with the previous method. It exhibits clear regional correlations in Australia, South Africa, western Europe and North America.

[51] Figure 4 displays the annual signals estimated for all colocated techniques. The significant annual signals for all other GPS stations are also shown. The annual signals measured by the three techniques are in agreement at a few colocated sites. The list of these sites is given in Table 5 together with their annual signal estimates. A few sites exhibit impressive agreement both in amplitude and phase, such as the Yarragadee, Canberra, Hobart and Hartebeesthoek sites. This agreement is reinforced by the spatial consistency of GPS annual signals fitted at the other regional sites; see the map of Australia in Figure 4. What can be clearly seen is that the three techniques reflect a common spatially correlated signal. As the three techniques are independent regarding their measurement principles, this agreement may be interpreted as evidence of an underlying geophysical signature. We consequently suggest this area, as well as the south of Africa and eastern North America for geodynamic investigation. The total contribution of the annual loading effects has been studied by *Mangiarotti et al.* [2001]. Plates 1 to 3 of *Mangiarotti et al.*, 2001], which present annual amplitude and phases of the total annual loading effect, can be compared to Figure 4. The case of sites in Europe is also instructive. The GPS annual signal in eastern Europe is spatially coherent. Matera VLBI station (Italy) seems to follow the phase of the motion and Potsdam SLR station (Germany) also although the estimated signal is less well determined. However, Wettzell (Germany) and Zimmerwald stations (Switzerland) do not exhibit agreement at that frequency. *van Dam et al.* [2007] have also compared IGS residual position time series after

having corrected them for the effect of atmosphere and ocean loads to their GRACE water loading displacement model. The agreement was also very poor notably at the coastal area.

[52] We observe for some residual time series, mainly GPS, very close spectral lines located near the annual frequency and its harmonics. Our interpretation of such spectral line groups is a time-varying behavior by the underlying periodic source. We have noticed that a second-order polynomial representation of the amplitude and phase of the annual signal approximates very well the signal, for example, for the GPS station MONP height time series.

4.3. Colocated Sites
4.3.1. Correlations

[53] Our method is illustrated using the results for Hartebeesthoek (South Africa). The estimated correlation between VLBI and GPS height time series is 0.88 ± 0.09 with comparable innovation variances, meaning that these two signals are very consistent. The smoothed GPS and VLBI daily height time series can be estimated with the help of the Kalman filter equations [*Gourieroux and Monfort*, 1997], theorem 15.5. The plot of these signals is shown in Figure 5a. The smoothed signals have comparable amplitudes and are very similar due to the important value of the correlation coefficient. The VLBI signal is much more smoothed than the GPS signal because the uncertainties of the original height time series are higher and moreover rescaled by a factor of 1.4. Figure 5a illustrates that this method can be used to interpolate a position time series in a colocated site when data are missing. The SLR and GPS signals for this site are also very consistent at the level of 0.68 ± 0.15 with comparable levels of variance (see Table 6).

[54] The results of site correlation estimates are computed for pairs of time series with more than 200 estimated positions in the common data period. The results are given in Table 6 for GPS and VLBI, for GPS and SLR and for VLBI and SLR comparisons, ordered by colocation site. We have observed unbalanced solutions when the numbers of data points of the two series are small or when the number of data points are not of the same order. This is the case for the Hobart comparison, see Table 7. The minimization algorithm has converged to null VLBI innovation variance for Tsukuba correlation estimation between VLBI and GPS time series and between VLBI and SLR data at Matera. The results of these comparisons have consequently been omitted in Table 6, since in that case, the correlation coefficient is not meaningful.

[55] The first general comment concerns the estimation of the measurement noise variance factors. The ratio between the VLBI and GPS error bar factors lies mostly between 3 and 4 whereas it is around 4 to 7 for SLR and GPS time series comparisons. The correlation study between VLBI and SLR confirms these values since the ratio between SLR and VLBI error bar factors is around 1.5. According to these values, ILRS and IVS standard deviations are optimistic but the network effect may add scatter in the height time series as seen in section 2.3. Our method seems to underevaluate the GPS variance factor. This is in fact an expected result because, compared to SLR and VLBI, the GPS background
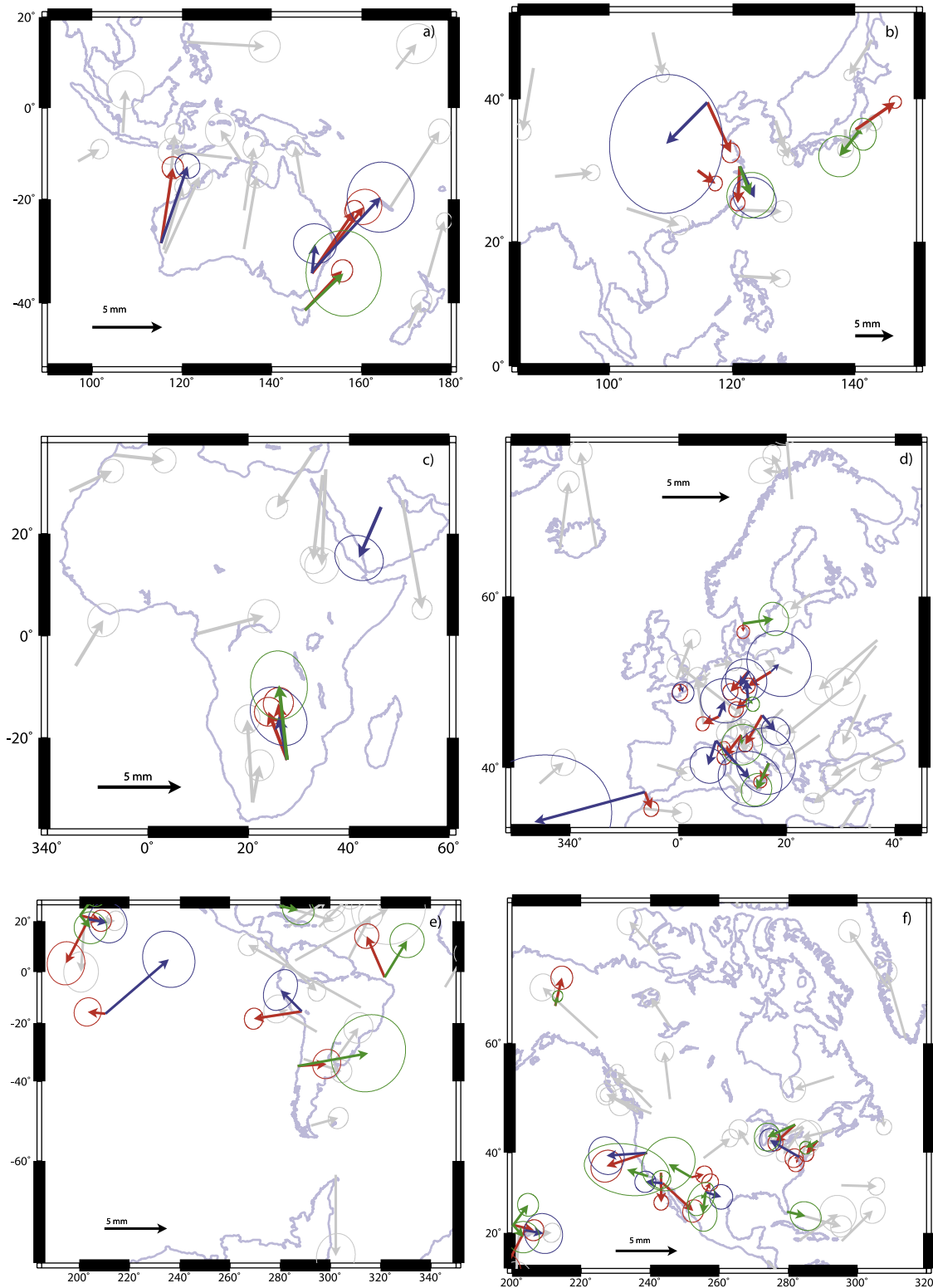
Figure 4. Vertical annual motions estimated for colocated GPS (red), VLBI (green), and SLR (blue) stations. Gray arrows represent the vertical annual motions for noncolocated GPS stations having SNR greater than 3.5. See Figure 3 for the plot conventions.

power spectrum is dominated by correlated noise processes. The measurement noise is assumed to be uncorrelated in our hypothesis; therefore the correlated part of the measurement noise is consequently absorbed in the GPS state height. The

correlation coefficients between GPS and VLBI lie between 0.5 and 0.9 with reasonable error bar values. Although VLBI state variances are always lower than GPS variances, probably because of GPS correlated measurement noise, the

Table 5. Nearly Consistent Annual Signals at Colocation Sites[a]

Site	Station	Technique	Amplitude, mm	Phase, deg
Matera	MATE	GPS	1.5 ± 0.2	205 ± 7
	7243	VLBI	2.2 ± 0.5	205 ± 12
Potsdam	POTS	GPS	2.1 ± 0.2	222 ± 6
	7836	SLR	1.4 ± 0.6	212 ± 23
Shanghai	SHAO	GPS	4.8 ± 0.4	183 ± 5
	7227	VLBI	4.0 ± 1.1	160 ± 18
	7837	SLR	4.5 ± 1.2	154 ± 14
Hartebeesthoek	HRAO	GPS	3.1 ± 0.3	339 ± 6
	7232	VLBI	4.5 ± 0.8	354 ± 9
	7501	SLR	2.7 ± 0.7	349 ± 14
Algonquin	ALGO	GPS	2.2 ± 0.3	228 ± 7
	7282	VLBI	2.5 ± 0.4	246 ± 10
Fairbanks	FAIR	GPS	2.4 ± 0.4	13 ± 9
	7225	VLBI	0.8 ± 0.2	14 ± 12
Quincy	QUIN	GPS	3.5 ± 0.5	252 ± 8
	7109	SLR	3.3 ± 0.6	266 ± 11
Westford	WES2	GPS	1.4 ± 0.2	221 ± 10
	7209	VLBI	1.1 ± 0.2	240 ± 11
Concepcion	CONZ	GPS	2.3 ± 0.5	86 ± 12
	7640	VLBI	5.7 ± 1.2	80 ± 12
Canberra	TIDB	GPS	5.4 ± 0.3	34 ± 3
	7843	SLR	7.2 ± 1.0	43 ± 8
Yarragadee	YAR2	GPS	5.4 ± 0.3	9 ± 3
	7090	SLR	5.8 ± 0.4	19 ± 4
Hobart	HOB2	GPS	3.9 ± 0.3	44 ± 5
	7242	VLBI	3.8 ± 1.1	46 ± 18

[a]The amplitude A and the phase ϕ values are provided with the convention $A \cos(\omega(t - 2000.0) - \phi)$.

innovation variances have comparable values with respect to their error bars. These results reflect the good consistency between GPS and VLBI heights at every colocated site with sufficient data. Figure 5d also displays IVS and IGS residual height time series as well as their smoothed values at Ny Alesund. We observe some periods of time when these two residual time series disagree.

[56] The SLR results are more disparate. SLR height standard deviations need to be rescaled by an average factor of 2. We notice that some sites have heterogeneous levels of variances for the GPS and SLR innovation processes. Figure 5c shows, for example, ILRS and IGS height residual time series at Wettzell (Europe) where this configuration is encountered. The consistency is achieved when these quantities are of the same order of magnitude with reasonable values of the correlation coefficient like at Hartebeesthoek, Potsdam, Arequipa, or Yarragadee (see Figure 5b).

[57] Unfortunately, the comparison of SLR and VLBI data is only possible for two colocated sites (see Table 6) because of a lack of common data. Contrary to Wettzell, Hartebeesthoek shows close agreement between VLBI and SLR. This colocated site exhibits consistent residual height time series for all three techniques whatever the time series being compared.

4.3.2. Interannual and Intra-annual Variations

[58] We focus in this part on the interannual variations by first assessing the extent to which the correlation coefficients in section 4.3.1 can be attributed to the annual signals. To answer this question, colocated sites with consistent detected annual signals are studied. A common annual signal is first fitted at every colocated site using VLBI, GPS and SLR data where at least a couple of fitted

annual signals are consistent. These data are weighted in the estimation process with the variance factor values estimated by MLE (see Table 6). As previously mentioned, the GPS variance factors from Table 6 are lower than those of the other techniques. The GPS signal will consequently dominate the estimated annual term. The combined annual values are given in Table 7. At each of these sites, the estimated signal is removed from the input data and a new correlation coefficient is estimated with the previous method for couple of time series having more than 200 points in their common data period. Results are shown in Table 7.

[59] The measurement noise standard deviation factors of all sites stay unchanged compared to Table 6. The innovation variances and correlation coefficients slightly decrease for most of the sites but do not decrease as much as we might have expected. The reason is that the time series scatter do not decrease so much when an annual wave is removed. Indeed, a single wave is not sufficient to represent the annual pattern being repeated in the time series, these being subject to significant interannual variations. Thus, for most of these sites, the annual signal spectral line is not the only one responsible for the consistency observed, notably between GPS and VLBI time series. The SLR and GPS time series comparison in Yarragadee demonstrates that SLR and GPS in this site have mainly a consistent annual signal and probably not more. Once removed, the correlation obtained, for equal state variances, is no longer significant.

5. Conclusion

[60] For the first time, combined input TRF time series of independent techniques have been analyzed homogeneously for the ITRF2005 computation. It is therefore a great opportunity to assess the agreement between the VLBI, GPS and SLR time series of positions. The key feature of such comparisons relies on colocated sites where instruments of different techniques operate close to each other.

[61] The residual height time series from a rigorous stacking have been compared using spectral and correlation analysis. However, the procedure used to estimate station stacked coordinates does not prevent aliasing which can occur between station individual motion and Helmert parameters that need to be estimated to remove global translation motions and biases. We have evaluated the network effect at the level of 1 mm for the IGS network. This value remains, however, somewhat questionable since it assumes that a well-distributed network does not suffer from the network effect. Thanks to simulations realized using ILRS and IVS colocated IGS stations, we have also evaluated the network effect at the level of 2 mm for height SLR time series and 3 mm for VLBI height time series. As previously mentioned by *Dong et al.* [1998] and *Lavallée et al.* [2006] and as checked here, the estimation of a scale parameter changes the residual time series quite significantly. It seems, however, that the introduction of this parameter affects quite similarly the residual height time series at the annual frequency. These values give an order of magnitude of the network effect but should be refined with more complex simulations using fully synthetic data integrating all stations with realistic synthetic noise processes. Although estimating the scale will still be useful to monitor the monotechnique frame stability, further studies need to be
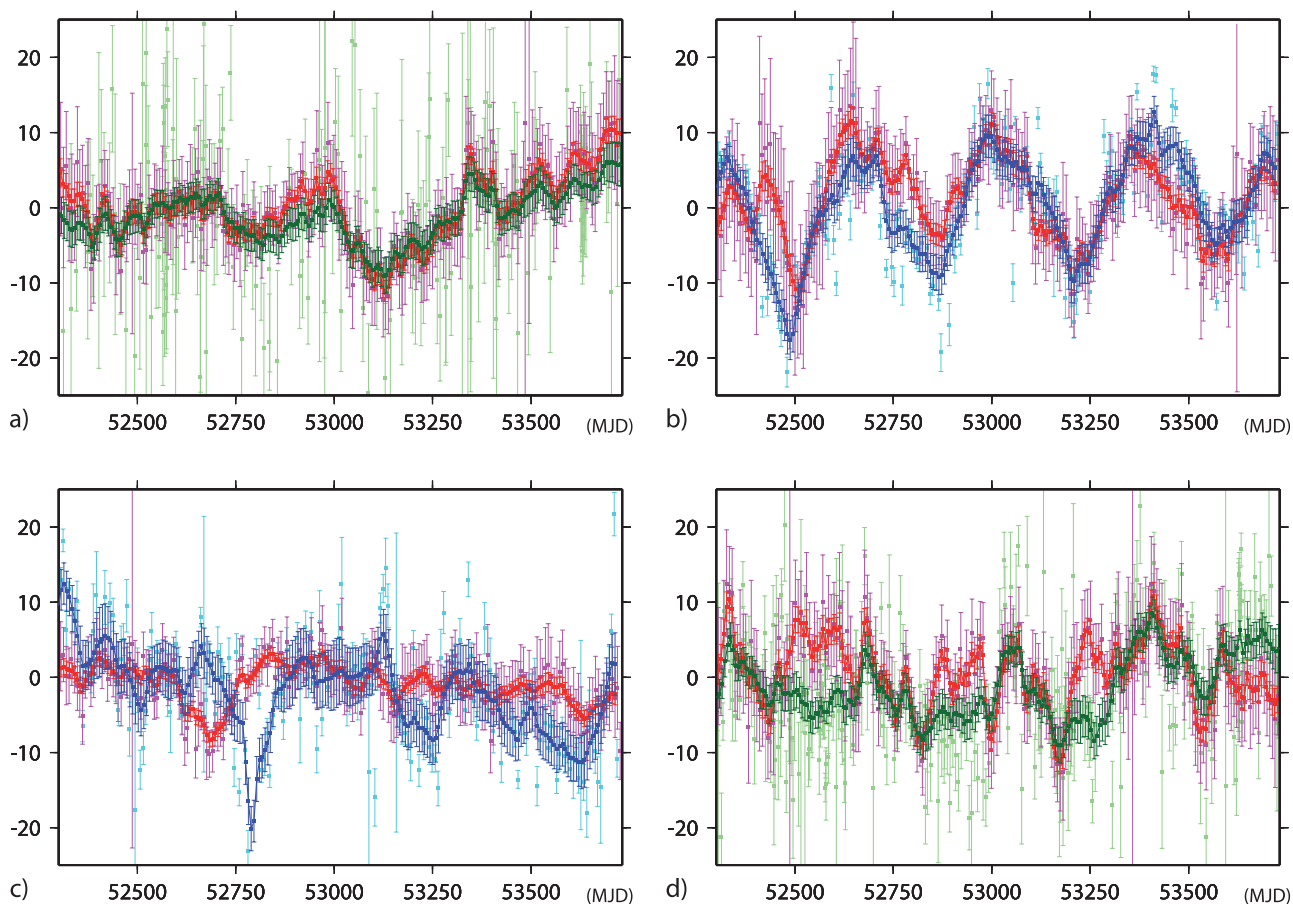
Figure 5. Height residual time series at four colocated sites (a) Hartebeesthoek, 7232 (VLBI) and HRAO (GPS); (b) Yarragadee: 7090 (SLR) and YAR2 (GPS); (c) Wettzell, 8834 (SLR) and WTZR (GPS); (d) Ny Alesund, 7331 (VLBI) and NYA1 (GPS). IGS, IVS, and ILRS height residual time series are plotted in magenta, light green, and cyan, respectively. Smoothed curves produced with estimated parameters of Table 6 are plotted over in solid red for GPS, dark green for VLBI, and solid blue for SLR.

made to analyze the utility of estimating the scale parameter in the stacking procedure for future realizations of the ITRS.

[62] We have developed a method of time series comparison, which solves in first approximation the sampling problem of the time series from VLBI and GPS or SLR. This method also takes into account the heterogeneity of the position quality using the formal errors provided with the technique residuals. The correlation coefficients are estimated at colocated sites and produce reasonable agreement in a number of cases. GPS and VLBI agree quite well for almost every site with sufficient data whereas good results are obtained for only a few SLR and GPS sites. According to our method, the Hartebeesthoek site has been demonstrated to exhibit agreement for the three techniques height time series.

[63] The spectral content of VLBI, GPS and SLR height residuals has also been investigated using the FAMOUS software [*Mignard*, 2005]. The annual spectral line has been detected in most height time series of all three techniques. The GPS annual signal is regionally correlated over some continental areas. Regarding the three techniques, this spatial correlation is confirmed for some areas like Australia, South Africa and eastern North America. As a

consequence, we suggest these areas for geodynamical investigation and model comparisons. No significant spectral lines at the semiannual signal in agreement with IGS height residuals have been found in IVS and ILRS height time series. IGS height time series also exhibit several spectral lines, close to the annual harmonics, notably around 3.09 and 4.14 cpy. The amplitude of these signals is typically less than 2 mm on the vertical. This study confirms the results of *Ray et al.* [2007] about anomalous harmonics present in the GPS position stacked periodograms.

[64] Some improvements in data modeling have been done during the ITRF2005 computation and validation period in the analysis of the three techniques observables. New mapping functions have been developed such as Vienna mapping function (VMF) and Vienna mapping function 1 (VMF1), which are shown to fit the VLBI data better than the Niell mapping functions [*Boehm et al.*, 2006b]. The use of VMF reveals some bias in the height components compared to NMF, mostly used for ITRF2005, and modifies the annual signal in heights [*Boehm et al.*, 2006b; *Tesmer et al.*, 2006]. Some studies have been made with GPS using the global mapping function (GMF) [*Boehm et al.*, 2006a], which has been fitted to the VMF.

Table 6. Innovation Standard Deviations σ_{wn1} and σ_{wn2}, Correlations ρ, and Error Bar Scaling Factors σ_{01} and σ_{02} Estimated for Pairs of Time Series[a]

Site	Station1	Station2	Type	σ_{wn1} mm	σ_{wn2} mm	ρ	σ_{01}	σ_{02}
Algonquin	7282 (516)	ALGO (507)	RP[b]	0.61 ± 0.10	0.68 ± 0.07	0.89 ± 0.07	1.21 ± 0.04	0.62 ± 0.03
Arequipa	7403 (255)	AREQ (340)	LP[c]	0.75 ± 0.12	0.98 ± 0.10	0.28 ± 0.19	2.23 ± 0.12	0.37 ± 0.03
Borowiec	7811 (335)	BOR1 (508)	LP	1.49 ± 0.26	0.74 ± 0.09	0.58 ± 0.14	3.26 ± 0.17	0.35 ± 0.02
Fairbanks	7225 (745)	FAIR (455)	RP	0.51 ± 0.12	0.78 ± 0.09	0.54 ± 0.16	1.65 ± 0.05	0.66 ± 0.03
Fort Davis	7080 (474)	MDO1 (512)	LP	0.91 ± 0.10	0.78 ± 0.07	0.20 ± 0.14	2.12 ± 0.09	0.36 ± 0.02
Grasse	7845 (263)	GRAS (325)	LP	1.19 ± 0.22	0.55 ± 0.08	−0.54 ± 0.19	2.44 ± 0.18	0.23 ± 0.02
	7835 (365)	GRAS (439)	LP	1.05 ± 0.17	0.70 ± 0.09	−0.07 ± 0.20	2.69 ± 0.15	0.19 ± 0.02
Hartebeesthoek	7232 (386)	HRAO (413)	RP	0.56 ± 0.13	0.79 ± 0.07	0.89 ± 0.09	1.19 ± 0.04	0.38 ± 0.02
	7501 (225)	HRAO (277)	LP	0.75 ± 0.14	0.66 ± 0.08	0.67 ± 0.14	2.92 ± 0.17	0.40 ± 0.03
	7232 (244)	7501 (225)	RL[d]	0.55 ± 0.18	0.76 ± 0.15	0.80 ± 0.14	1.22 ± 0.06	2.89 ± 0.17
Herstmonceux	7840 (498)	HERS (298)	LP	0.26 ± 0.33	0.67 ± 0.08	0.47 ± 0.65	3.31 ± 0.32	0.27 ± 0.02
Hobart	7242 (201)	HOB2 (475)	RP	0.38 ± 0.18	0.64 ± 0.05	0.97 ± 0.06	1.15 ± 0.06	0.45 ± 0.02
Kauai	7298 (841)	KOKB (495)	RP	0.51 ± 0.08	1.01 ± 0.08	0.54 ± 0.15	1.49 ± 0.04	0.51 ± 0.03
Matera	7243 (326)	MATE (503)	RP	0.44 ± 0.10	0.55 ± 0.05	0.84 ± 0.13	1.48 ± 0.06	0.33 ± 0.02
Monument Peak	7110 (455)	MONP (479)	LP	0.65 ± 0.09	0.99 ± 0.08	−0.09 ± 0.14	2.90 ± 0.12	0.17 ± 0.01
Ny-Alesund	7331 (503)	NYA1 (394)	RP	0.78 ± 0.15	1.03 ± 0.10	0.68 ± 0.13	1.78 ± 0.07	0.39 ± 0.03
	7331 (597)	NYAL (486)	RP	0.66 ± 0.13	1.32 ± 0.11	0.55 ± 0.14	1.79 ± 0.11	0.30 ± 0.02
Potsdam	7836 (346)	POTS (428)	LP	0.76 ± 0.13	0.66 ± 0.08	0.30 ± 0.22	2.01 ± 0.10	0.44 ± 0.03
San Fernando	7824 (239)	SFER (341)	LP	3.75 ± 0.49	0.58 ± 0.06	0.35 ± 0.17	2.93 ± 0.20	0.29 ± 0.02
Shanghai	7837 (283)	SHAO (332)	LP	1.54 ± 0.29	0.96 ± 0.09	0.08 ± 0.20	3.27 ± 0.20	0.32 ± 0.02
Washington	7105 (473)	GODE (509)	LP	1.42 ± 0.20	0.80 ± 0.10	0.52 ± 0.13	2.39 ± 0.17	0.31 ± 0.02
	7105 (405)	USNO (439)	LP	1.53 ± 0.22	0.66 ± 0.08	0.53 ± 0.13	2.41 ± 0.19	0.42 ± 0.03
Westford	7209 (528)	WES2 (498)	RP	0.40 ± 0.09	0.54 ± 0.06	0.61 ± 0.16	1.67 ± 0.06	0.41 ± 0.02
Wettzell	7224 (964)	WTZR (503)	RP	0.37 ± 0.10	0.48 ± 0.05	0.81 ± 0.09	1.60 ± 0.04	0.53 ± 0.03
	8834 (417)	WTZR (500)	LP	1.19 ± 0.15	0.42 ± 0.05	0.11 ± 0.17	2.97 ± 0.15	0.54 ± 0.03
	7224 (1253)	8834 (560)	RL	0.17 ± 0.06	1.35 ± 0.16	0.13 ± 0.37	1.60 ± 0.03	3.05 ± 0.13
Yarragadee	7090 (498)	YAR2 (497)	LP	0.92 ± 0.09	0.84 ± 0.06	0.46 ± 0.10	3.37 ± 0.15	0.38 ± 0.02
Zimmerwald	7810 (355)	ZIMM (439)	LP	0.95 ± 0.14	0.48 ± 0.05	−0.18 ± 0.17	2.92 ± 0.15	0.28 ± 0.02

[a]See equations (3) and (5). The number of estimated positions considered for each station is indicated between brackets.
[b]VLBI-GPS.
[c]SLR-GPS.
[d]VLBI-SLR.

The same conclusions have been addressed by *Boehm et al.* [2005], although that study tested only 1 year of data. The elevation cutoff angle used by the authors was, however, smaller than the one currently used by the IGS ACs. The use of global pressure and temperature models to compute a priori zenith delays has been shown to reduce spurious annual signals in the GPS analysis as demonstrated by *Tregoning and Herring* [2006]. Similarly, SLR analyses will benefit from improved zenith delays with the M-P model [*Mendes and Pavlis*, 2004]. *Hulley and Pavlis* [2007] also give some perspectives for improving SLR analysis using horizontal refractivity gradients computed from external data sets to model the tropospheric delay. A study led by *Wresnik et al.* [2007] has shown new perspectives in the modeling of the thermal deformation of the VLBI telescopes. These results are encouraging for the modeling of

Table 7. Innovation Standard Deviations σ_{wn1} and σ_{wn2}, Correlations ρ, and Error Bar Scaling Factors σ_{01} and σ_{02} Estimated for Pairs of Time Series After a Common Annual Signal Has Been Removed[a]

Site	Station 1	Station 2	Type	A mm	ϕ deg	σ_{wn1} mm	σ_{wn2} mm	ρ	σ_{01}	σ_{02}
Algonquin	7282 (516)	ALGO (507)	RP[b]	2.1 ± 0.2	230 ± 5	0.50 ± 0.11	0.65 ± 0.07	0.87 ± 0.08	1.22 ± 0.05	0.62 ± 0.04
Fairbanks	7225 (745)	FAIR (455)	RP	1.6 ± 0.2	15 ± 5	0.40 ± 0.10	0.72 ± 0.08	0.42 ± 0.21	1.67 ± 0.05	0.67 ± 0.03
Hartebe-	7232 (386)	HRAO (413)	RP	3.0 ± 0.2	340 ± 4	0.35 ± 0.13	0.75 ± 0.07	0.75 ± 0.24	1.19 ± 0.05	0.38 ± 0.02
esthoek	7501 (225)	HRAO (277)	LP[c]			0.61 ± 0.15	0.59 ± 0.09	0.53 ± 0.20	2.94 ± 0.18	0.41 ± 0.03
Hobart	7242 (201)	HOB2 (475)	RP	4.0 ± 0.2	45 ± 3	0.05 ± 0.12	0.52 ± 0.05	0.60 ± 1.88	1.13 ± 0.06	0.44 ± 0.02
Matera	7243 (326)	MATE (503)	RP	1.9 ± 0.2	198 ± 5	0.31 ± 0.11	0.49 ± 0.05	0.72 ± 0.23	1.48 ± 0.06	0.33 ± 0.02
Potsdam	7836 (346)	POTS (429)	LP	2.0 ± 0.2	220 ± 7	0.71 ± 0.12	0.63 ± 0.08	0.16 ± 0.25	2.03 ± 0.10	0.45 ± 0.03
Shanghai	7837 (283)	SHAO (332)	LP	4.5 ± 0.4	181 ± 5	1.44 ± 0.28	0.84 ± 0.09	−0.13 ± 0.23	3.31 ± 0.20	0.33 ± 0.02
Westford	7209 (528)	WES2 (498)	RP	1.3 ± 0.2	228 ± 6	0.35 ± 0.10	0.51 ± 0.06	0.58 ± 0.18	1.68 ± 0.06	0.42 ± 0.02
Yarragadee	7090 (498)	YAR2 (497)	LP	5.5 ± 0.2	13 ± 2	0.69 ± 0.10	0.72 ± 0.06	0.23 ± 0.14	3.49 ± 0.15	0.39 ± 0.02

[a]The amplitude and phase of the annual term are provided with respect to the model $A \cos(\omega(t - 2000.0) - \phi)$. The number of estimated positions considered for each station is indicated between brackets.
[b]VLBI-GPS.
[c]SLR-GPS.

this effect at the observational level if their generalization is possible. It will be valuable for future work to study homogeneously processed GPS position time series [*Steigenberger et al.*, 2006]. The analysis and interpretation of low-frequency signals would be worth doing.

[65] We may consequently expect the agreement to become better in the near future when the data of the three techniques will have been homogeneously reprocessed using new models.

[66] **Acknowledgments.** This research was carried out at the Laboratoire de Recherche en Géodésie (LAREG) within the Institut Géographique National (IGN) of France. The authors thank Tonie van Dam and François Mignard for fruitful discussions and also thank the ILRS, IGS, and IVS for providing their solutions. The valuable comments of the reviewers D. Lavallée and S. Wdowinski are gratefully acknowledged. All the plots have been made with the General Mapping Tool (GMT) software, available at http://gmt.soest.hawaii.edu/ under the GNU General Public Licence.

References

Altamimi, Z., P. Sillard, and C. Boucher (2002), ITRF2000: A new release of the International Terrestrial Reference Frame for earth science applications, *J. Geophys. Res.*, *107*(B10), 2214, doi:10.1029/2001JB000561.

Altamimi, Z., X. Collilieux, and C. Boucher (2006), Accuracy assessment of the ITRF datum definition, paper presented at V Hotine-Marussi Symposium on Mathematical Geodesy IAG Symposia, Int. Assoc. of Geod., Wuhan, China.

Altamimi, Z., X. Collilieux, J. Legrand, B. Garayt, and C. Boucher (2007), ITRF2005: A new release of the International Terrestrial Reference Frame based on time series of station positions and Earth Orientation Parameters, *J. Geophys. Res.*, *112*, B09401, doi:10.1029/2007JB004949.

Blewitt, G., and D. Lavallée (2000), Effect of annually repeating signals on geodetic velocity estimates, paper presented at The Tenth General Assembly of the WEGENER Project (WEGENER 2000), San Fernando, Spain, 18–20 Sept.

Blewitt, G., and D. Lavallée (2002), Effect of annual signals on geodetic velocity, *J. Geophys. Res.*, *107*(B7), 2145, doi:10.1029/2001JB000570.

Boehm, J., A. Mendes Cerveira, P. Tregoning, and H. Schuh (2005), The impact of tropospheric mapping functions based on numerical weather models on the determination of geodetic parameters, paper presented at IAG meeting, Int. Assoc. of Geod., Cairns, Australia.

Boehm, J., A. Niell, P. Tregoning, and H. Schuh (2006a), Global Mapping Function (GMF): A new empirical mapping function based on numerical weather model data, *Geophys. Res. Lett.*, *33*, L07304, doi:10.1029/2005GL025546.

Boehm, J., B. Werl, and H. Schuh (2006b), Troposphere mapping functions for GPS and very long baseline interferometry from European Centre for Medium-Range Weather Forecasts operational analysis data, *J. Geophys. Res.*, *111*, B02406, doi:10.1029/2005JB003629.

Chambodut, A., I. Panet, M. Mandea, M. Diament, M. Holschneider, and O. Jamet (2005), Wavelet frames: An alternative to spherical harmonic representation of potential fields, *Geophys. J. Int.*, *163*, 875–899, doi:10.1111/j.1365-246X.2005.02754.x.

Ding, X. L., D. W. Zheng, D. N. Dong, C. Ma, Y. Q. Chen, and G. L. Wang (2005), Seasonal and secular positional variations at eight co-located GPS and VLBI stations, *J. Geod.*, *79*, 71–81, doi:10.1007/s00190-005-0444-3.

Dong, D., T. A. Herring, and R. W. King (1998), Estimating regional deformation from a combination of space and terrestrial geodetic data, *J. Geod.*, *72*, 200–214.

Dong, D., P. Fang, Y. Bock, M. K. Cheng, and S. Miyazaki (2002), Anatomy of apparent seasonal variations from GPS-derived site position time series, *J. Geophys. Res.*, *107*(B4), 2075, doi:10.1029/2001JB000573.

Farrell, W. E. (1972), Deformation of the Earth by surface loads, *Rev. Geophys.*, *10*, 761–797.

Ferland, R. (2003), Reference frame working group technical report, 2001–2002 technical report, *Tech. rep.*, Int. GNSS Serv., Pasadena, Calif.

Ferland, R., and D. Hutchison (2001), IGSREPORT-8898, Wk 1144 IGS SINEX Combination, techical report, Int. GNSS Serv., LOCATION.

Gourieroux, C., and A. Monfort (1997), *Time Series and Dynamic Models*, Cambridge Univ. Press, New York.

Hamilton, J. D. (1994), *Time Series Analysis*, Princeton Univ. Press, Princeton, N. J.

Herring, T. A., J. L. Davis, and I. I. Shapiro (1990), Geodesy by radio interferometry: The application of Kalman filtering to the analysis of very long baseline interferometry data, *J. Geophys. Res.*, *95*, 12,561–12,581.

Hulley, G. C., and E. C. Pavlis (2007), A ray-tracing technique for improving Satellite Laser Ranging atmospheric delay corrections, including the effects of horizontal refractivity gradients, *J. Geophys. Res.*, *112*, B06417, doi:10.1029/2006JB004834.

Langbein, J., and H. Johnson (1997), Correlated errors in geodetic time series: Implications for time-dependent deformation, *J. Geophys. Res.*, *102*, 591–604.

Lavallée, D. A., T. van Dam, G. Blewitt, and P. J. Clarke (2006), Geocenter motions from GPS: A unified observation model, *J. Geophys. Res.*, *111*, B05405, doi:10.1029/2005JB003784.

Le Bail, K., J. Valette, W. Zerhouni, and M. Feissel-Vernier (2007), Long-term consistency of multi-technique terrestrial reference frames, a spectral approach, in *Dynamic Planet: Monitoring and Understanding a Dynamic Planet with Geodetic and Oceanographic Tools*, *Int. Assoc. Geod. Symp.*, vol. 130, edited by P. Tregoning and C. Rizos, pp. 692–700, Springer, New York.

Luceri, V., and E. Pavlis (2006), The ILRS solution, technical report, ILRS technical report, Int. Laser Rang. Serv., Greenbelt, Md.

Mangiarotti, S., A. Cazenave, L. Soudarin, and J. F. Crétaux (2001), Annual vertical crustal motions predicted from surface mass redistribution and observed by space geodesy, *J. Geophys. Res.*, *106*, 4277–4292.

Mao, A., C. G. A. Harrison, and T. H. Dixon (1999), Noise in GPS coordinate time series, *J. Geophys. Res.*, *104*, 2797–2816.

McCarthy, D. D., and G. Petit (2004), IERS conventions (2003), *IERS Tech. Note 32*, Int. Earth Rotation and Ref. Syst. Serv., Frankfurt am Main, Germany.

Mendes, V. B., and E. C. Pavlis (2004), High-accuracy zenith delay prediction at optical wavelengths, *Geophys. Res. Lett.*, *31*, L14602, doi:10.1029/2004GL020308.

Mignard, F. (2005), Famous, frequency analysis mapping on usual sampling, technical report, Obs. de la Cote d'Azur Cassiopée, Nice, France.

Petrov, L., and J.-P. Boy (2004), Study of the atmospheric pressure loading signal in very long baseline interferometry observations, *J. Geophys. Res.*, *109*, B03405, doi:10.1029/2003JB002500.

Petrov, L., and C. Ma (2003), Study of harmonic site position variations determined by very long baseline interferometry, *J. Geophys. Res.*, *108*(B4), 2190, doi:10.1029/2002JB001801.

Press, W. H., S. A. Teukolsky, W. T. Vetterling, and B. P. Flannery (1996), *Numerical Recipes in FORTRAN 77: The Art of Scientific Computing*, 2nd ed., pp. 266–281, Cambridge Univ. Press, New York.

Ray, J. R., Z. Altamimi, X. Collilieux, and T. M. van Dam (2007), Anomalous harmonics in the spectra of GPS position estimates, *GPS Solutions*, doi:10.1007/s10291-007-0067-7, in press.

Scargle, J. D. (1982), Studies in astronomical time series analysis. II. Statistical aspects of spectral analysis of unevenly spaced data, *Astrophysical Journal*, *263*, 835–853.

Steigenberger, P., M. Rothacher, R. Dietrich, M. Fritsche, A. Rülke, and S. Vey (2006), Reprocessing of a global GPS network, *J. Geophys. Res.*, *111*, B05402, doi:10.1029/2005JB003747.

Stewart, M. P., N. T. Penna, and D. D. Lichti (2005), Investigating the propagation mechanism of unmodelled systematic errors on coordinate time series estimated using least squares, *J. Geod.*, *79*, 479–489, doi:10.1007/s00190-005-0478-6.

Tesmer, V., J. Boehm, R. Heinkelmann, and H. Schuh (2006), Impact of analysis options on the TRF, CRF and position time series estimated from VLBI, in *IVS 2006 General Meeting Proceedings*, *NASA Conf. Publ., NASA/CP-2006-214140*, 243–251.

Tesmer, V., J. Boehm, R. Heinkelmann, and H. Schuh (2007), Effect of different tropospheric mapping functions on the TRF, CRF and position time-series estimated from VLBI, *J. Geod.*, *81*, 409–421, doi:10.1007/s00190-006-0126-9.

Titov, O., and H. Yakovleva (1999), Seasonal variation in radial components of VLBI stations, *Astron. Astrophys. Trans.*, *18*, 593–606.

Tregoning, P., and T. A. Herring (2006), Impact of a priori zenith hydrostatic delay errors on GPS estimates of station heights and zenith total delays, *Geophys. Res. Lett.*, *33*, L23303, doi:10.1029/2006GL027706.

Tregoning, P., and T. van Dam (2005), Effects of atmospheric pressure loading and seven-parameter transformations on estimates of geocenter motion and station heights from space geodetic observations, *J. Geophys. Res.*, *110*, B03408, doi:10.1029/2004JB003334.

van Dam, T. M., and T. A. Herring (1994), Detection of atmospheric pressure loading using very long baseline interferometry measurements, *J. Geophys. Res.*, *99*, 4505–5417.

van Dam, T., J. Wahr, P. C. D. Milly, A. B. Shmakin, G. Blewitt, D. Lavallée, and K. M. Larson (2001), Crustal displacements due to continental water loading, *Geophys. Res. Lett.*, *28*, 651–654.

van Dam, T., J. Wahr, and D. Lavalle (2007), A comparison of annual vertical crustal displacements from GPS and Gravity Recovery and Climate Experiment (GRACE) over Europe, *J. Geophys. Res.*, *112*, B03404, doi:10.1029/2006JB004335.

van Dam, T. M., G. Blewitt, and M. B. Heflin (1994), Atmospheric pressure loading effects on Global Positioning System coordinate determinations, *J. Geophys. Res.*, *99*, 23,939–23,950.

Vennebusch, M., S. Böckmann, and A. Nothnagel (2006), The contribution of very long baseline interferometry to ITRF2005, *J. Geod.*, *81*, 553–564, doi:10.1007/s00190-006-0117-x.

Williams, S. D. P., Y. Bock, P. Fang, P. Jamason, R. M. Nikolaidis, L. Prawirodirdjo, M. Miller, and D. J. Johnson (2004), Error analysis of continuous GPS position time series, *J. Geophys. Res.*, *109*, B03412, doi:10.1029/2003JB002741.

Wresnik, J., R. Haas, J. Boehm, and H. Schuh (2007), Modeling thermal deformation of VLBI antennas with a new temperature model, *J. Geod.*, *81*, 423–431, doi:10.1007/s00190-006-0120-2.

Zhang, J., Y. Bock, H. Johnson, P. Fang, S. Williams, J. Genrich, S. Wdowinski, and J. Behr (1997), Southern California Permanent GPS Geodetic Array: Error analysis of daily position estimates and site velocities, *J. Geophys. Res.*, *102*, 18,035–18,056.

————————————

Z. Altamimi, X. Collilieux, and D. Coulot, Laboratoire de Recherche en Géodésie/Institut Géographique National, 6-8 Avenue Blaise Pascal, Cité Descartes-Champs-sur-Marne, F-77455 Marne-La-Vallée Cedex 2, France. (xavier.collilieux@ign.fr)

J. Ray, NOAA National Geodetic Survey, N/NGS6, 1315 East-West Highway, Silver Spring, MD 20910, USA.

P. Sillard, Institut National de la Statistique et des Etudes Economiques, 15 Boulevard Gabriel Peri, BP 100, F-92244 MALAKOFF, cedex, France.